

RADIATIVELY SUSTAINED PLASMAS FOR SOLAR-ELECTRIC CONVERSION

AMES
7N-44-CR

Jay Palmer

**Hughes Research Laboratories
3011 Malibu Canyon Road
Malibu, CA 90265**

August 1979

NAS 2-10001

Annual Report

For period 1 July 1978 through 30 June 1979

Sponsored by

NATIONAL AERONAUTICS AND SPACE ADMINISTRATION

Ames Research Center

Moffett Field, CA 94035

(NASA-CR-182769) RADIATIVELY SUSTAINED
PLASMAS FOR SOLAR-ELECTRONIC CONVERSION
Annual Report, 1 Jul. 1978 - 30 Jun. 1979
(Hughes Research Labs.) 53 p

N90-70583

00/75 Unclass
0198808

#198808

TECHNICAL REPORT STANDARD TITLE PAGE

1. Report No.	2. Government Accession No.	3. Recipient's Catalog No.	
4. Title and Subtitle RADIATIVELY SUSTAINED PLASMAS FOR SOLAR-ELECTRIC CONVERSION		5. Report Date August 1979	
		6. Performing Organization Code	
7 Author(s) Jay Palmer		8. Performing Organization Report No.	
9. Performing Organization Name and Address Hughes Research Laboratories 3011 Malibu Canyon Road Malibu, CA 90265		10. Work Unit No.	
		11. Contract or Grant No. NAS 2-10001	
12. Sponsoring Agency Name and Address NATIONAL AERONAUTICS AND SPACE ADMINISTRATION AMES RESEARCH CENTER Moffett Field, CA 94035		13. Type of Report and Period Covered Annual Report 1 July 1978-30 June 1979	
		14. Sponsoring Agency Code	
15. Supplementary Notes			
16. Abstract <p>The first year's results of an experimental and theoretical study of solar-sustained cesium plasmas for solar-electric conversion and solar-pumped lasers are reported. A major upgrading of the original theoretical model describing the coupling of solar radiation to a cesium plasma was completed. The model now accounts for absorption by cesium dimers on four ground-to-excited-state transitions, for thermal convection and thermal conduction in the plasma, and for convergence of the input radiation in the plasma. For the parameters of the present experiments, the model predicts plasma maintenance at a plasma temperature of 2800°K and predicts the characteristic emission and absorption spectra of the plasma. Absorption spectra of cesium vapor at 600°C were experimentally measured, but window fogging and breakage problems made it necessary to redesign the cesium absorption cell as a heat pipe oven. The latest heat pipe oven cell fabricated should be capable of providing a 600 to 700°C zone of cesium vapor centered between windows that can be kept cold and that are isolated from the cesium vapor by helium buffer gas. The speculation that laser action on the Cs₂ and CsXe dimer and excimer laser transitions could be made to occur by flowing a solar-sustained cesium plasma through a transverse magnetic field has been confirmed theoretically with a quantitative model. An MHD flow model predicts gain coefficients greater than 1% per cm on both the excimer and dimer bands for a Mach 4 flow of a 10-atm solar-sustained CsXe plasma across an ~20-kG magnetic field.</p>			
17. Key Words (Selected by Author(s)) Solar-electric converters Solar-sustained plasmas Solar-pumped lasers		18. Distribution Statement	
19. Security Classif. (of this report) UNCLASSIFIED	20. Security Classif. (of this page) UNCLASSIFIED	21. No. of Pages 67	22. Price*

*For sale by the Clearinghouse for Federal Scientific and Technical Information, Springfield, Virginia 22151.

TABLE OF CONTENTS

SECTION		PAGE
	LIST OF ILLUSTRATIONS	5
1	INTRODUCTION	7
2	PLASMA MAINTENANCE — THEORETICAL	9
3	PLASMA MAINTENANCE — EXPERIMENTAL	19
4	SOLAR-PUMPED MHD LASER — THEORETICAL	33
5	FUTURE WORK	43
	APPENDIX A — Radiatively Sustained Cesium Plasmas for Solar Electric Conversion	47
	APPENDIX B — Flow Chart and Program Listing for Solar Sustained Plasma Model	59

LIST OF ILLUSTRATIONS

FIGURE		PAGE
1	Computed and measured absorption cross sections of cesium vapor: 0.40 to 0175 μm (measured values are from Ref. 4)	10
2	Computed and measured absorption cross sections of cesium vapor: 0.74 to 1.00 μm (measured values are from Ref. 4)	11
3	Theoretical solar flux required for sustaining a cesium plasma against radiation losses only	12
4	Theoretical solar-sustained plasma re-radiation spectrum (minus line emission)	14
5	Theoretical plasma temperature as a function of oven temperature showing radiation- and conduction-loss-dominated regimes	15
6	Theoretical plasma temperature as a function of distance from the front boundary of the vapor for two focal spot positions	17
7	Experimental set-up utilizing arc lamp solar simulator	20
8	Experimental set-up utilizing solar concentrator heliostat	21
9	Original ILC Corp. cesium absorption cell design	22
10	Cesium resonance line absorption	24
11	High-temperature cesium absorption spectra under partial illumination from the solar concentrator (a,b) and under full $\sim 377\text{-W}$ illumination from the concentrator (c,d)	25
12	Cracked entrance window of ILC absorption cell	27
13	First heat pipe oven design for solar-sustained plasma absorption cell	28
14	Photograph of first heat pipe oven absorption cell	29

FIGURE		PAGE
15	Photograph of latest heat pipe oven absorption cell	31
16	CsXe excimer and Cs ₂ dimer laser transitions	34
17	Theoretical electron and gas temperature versus mach number for solar-sustained plasma flow across a magnetic field	37
18	Theoretical gain coefficients and required magnetic field strength for solar-sustained plasma flow across a magnetic field	40

SECTION 1

INTRODUCTION

This report covers the first year's progress on a program devoted to the study of radiatively sustained cesium plasmas for solar-electric and solar-laser power conversion. The identification of a solar-sustained cesium plasma as an optimal high-temperature working fluid for solar electric conversion together with a preliminary theoretical model of the coupling of solar radiation to a cesium plasma was originally disclosed at the Third Conference on Radiation Energy Conversion at NASA Ames Research Center in 1978 and published in Progress in Astronautics and Aeronautics.¹ This paper is included as Appendix A.

The two primary objectives of this program are to (1) demonstrate experimentally the maintenance of a cesium plasma by solar radiation and to (2) make a firm prediction of the conditions necessary to achieve laser action on the Cs_2 dimer and CsXe excimer laser bands in such a plasma. A general updating of the theoretical model describing the coupling of solar radiation to a cesium plasma will also be done during this program. Progress on all three fronts was made during this contract period and is described below.

SECTION 2

PLASMA MAINTENANCE — THEORETICAL

The original theoretical model,¹ which predicted that a 3000°K cesium plasma could be ignited and maintained by concentrated sunlight, is presented in Appendix A. Similar modeling has been carried out for a solar-sustained potassium plasma.²

A major upgrading of the original theoretical model of a solar-sustained cesium plasma was found necessary primarily because of the need to account more accurately for dimer absorption in the 4000 to 8000 Å spectral range. Rather than computing the dimer absorption by simply inputting the measured values of the dimer absorption cross section at an arbitrary temperature (as done, for example, in Ref. 3), we chose to compute the temperature-dependent absorption cross sections according to a four-Morse-potential state model of the cesium dimer molecule. Not only does this allow accounting for the temperature dependence of the cross section, it also assures that re-radiation is accounted for properly on the dimer transitions. The 8,000 to 10,000 Å X-A absorption band can be modeled fairly exactly in this way since it is due to transition to a single state. And although the shorter wavelength bands are actually caused by several overlapping transitions, the absorption can be modeled to an accuracy sufficient for our purposes by constructing three hypothetical Morse potential states with the parameters given in Table 1. Our computed absorption cross sections (shown in Figures 1 and 2) agree well with Weschler's measured values.⁴ Line absorption is not included in the theoretical model since it contributes negligibly to the net energy flow in the plasma.

The corresponding new radiative energy balance results for a solar-sustained cesium plasma are shown in Figure 3. As shown, higher plasma temperatures result at lower oven temperatures in the purely radiative energy balance case because the lower fractional concentration of dimers causes the spectral range over which most of the absorption occurs to move to the shorter wavelengths associated with the bound-free transitions.¹

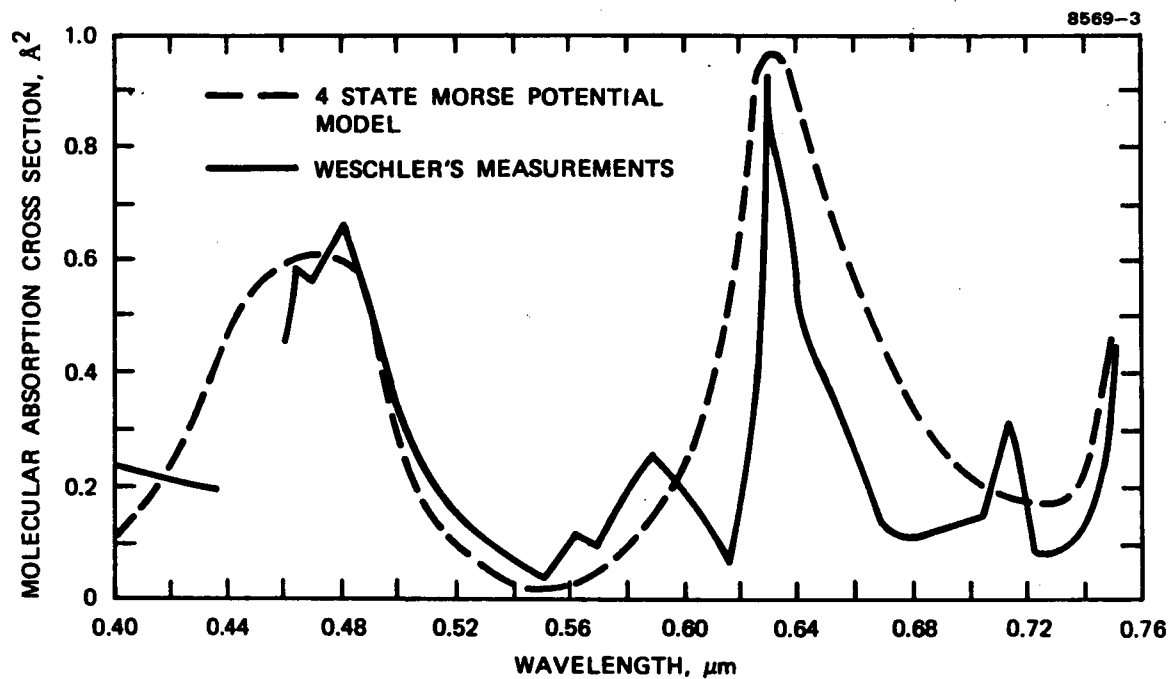


Figure 1. Computed and measured absorption cross sections of cesium vapor: 0.40 to 0.75 μm (measured values are from Ref. 4).

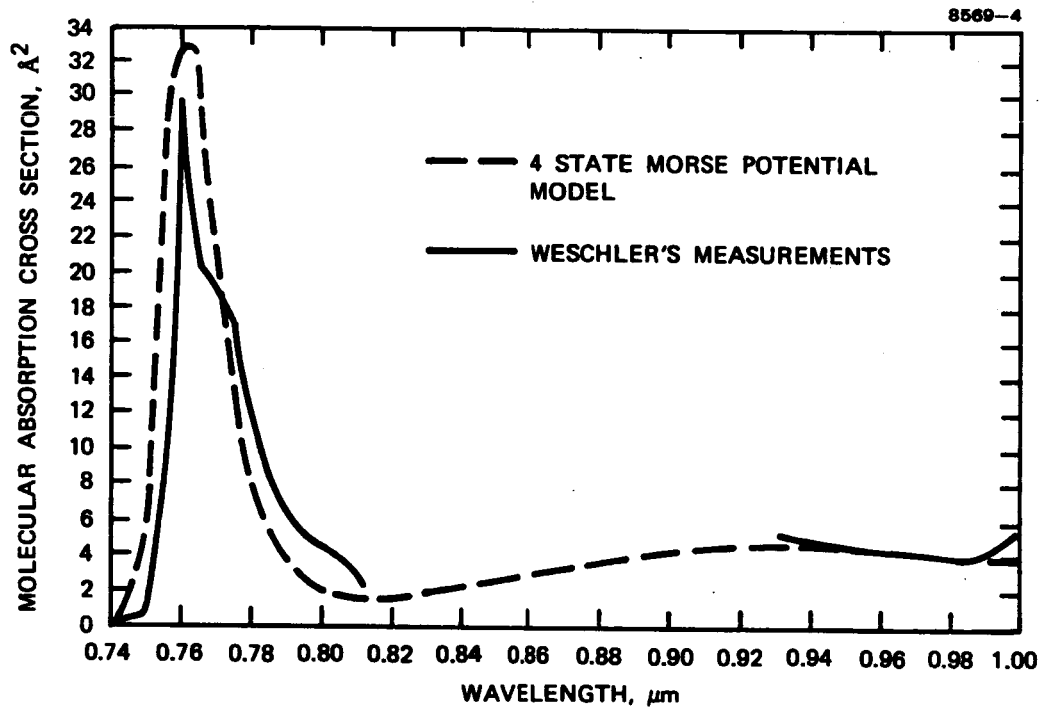


Figure 2. Computed and measured absorption cross sections of cesium vapor: 0.74 to 1.00 μm (measured values are from Ref. 4).

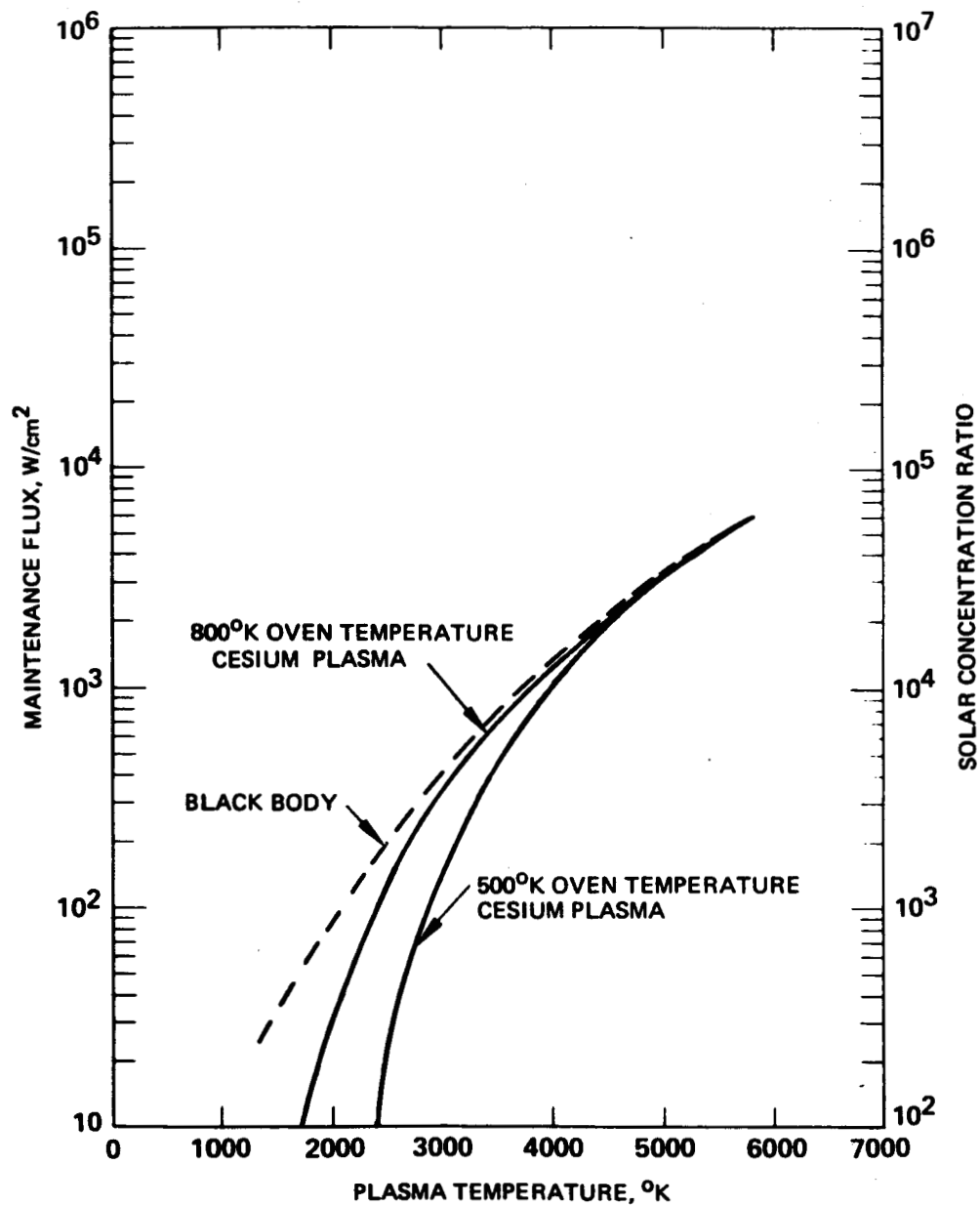


Figure 3. Theoretical solar flux required for sustaining a cesium plasma against radiation losses only.

Table 1. Morse Potential Parameters for the Four-State Model of Cs_2 Absorption Spectra

State	D, cm^{-1}	$R_e, \text{\AA}$	W_e, cm^{-1}	Atomic State
X	3600	4.47	42	6S
A	5100	5.25	34	6P 1/2
B	1510	4.47	34.2	6P 1/2
C	500	5.7	15	6P 3/2
E	5239	5.7	30	7P

6731

The addition of the visible dimer transitions has also enabled us to compute more accurately the emission spectra of the plasma under solar-sustained conditions. This is one of the most useful signatures to use for verifying plasma ignition in the experiments. A typical result is shown in Figure 4. Although line emission will of course also be present, it again is excluded from the model because it does not contribute importantly to the net energy flow in the plasma. Recombination radiation is seen to dominate dimer radiation in the visible portion of the spectrum for the conditions assumed.

Lower oven temperatures result in reduced radiative energy deposition in the plasma, which will eventually make losses other than radiation dominate the energy loss from the plasma. Therefore, we have added both thermal conduction and free convection losses to the model. For the densities, convection velocities, and dimensional scales of the present experiments, the estimated Reynolds number for the plasma is quite small (~ 100) permitting the use of a kinematic value for the thermal conductivity coefficient for cesium vapor ($\sim 15.1 \times 10^{-5} \text{ W/cm}^2\text{K}$).⁵ Since the free convection flow was not viscosity limited for the dimensional scale of the present experiments, it was computed from buoyancy forces alone.⁶ These nonradiative losses control the dependence of the plasma temperature on vapor pressure in our experiments for oven temperatures below about 800°K , as shown in Figure 5.

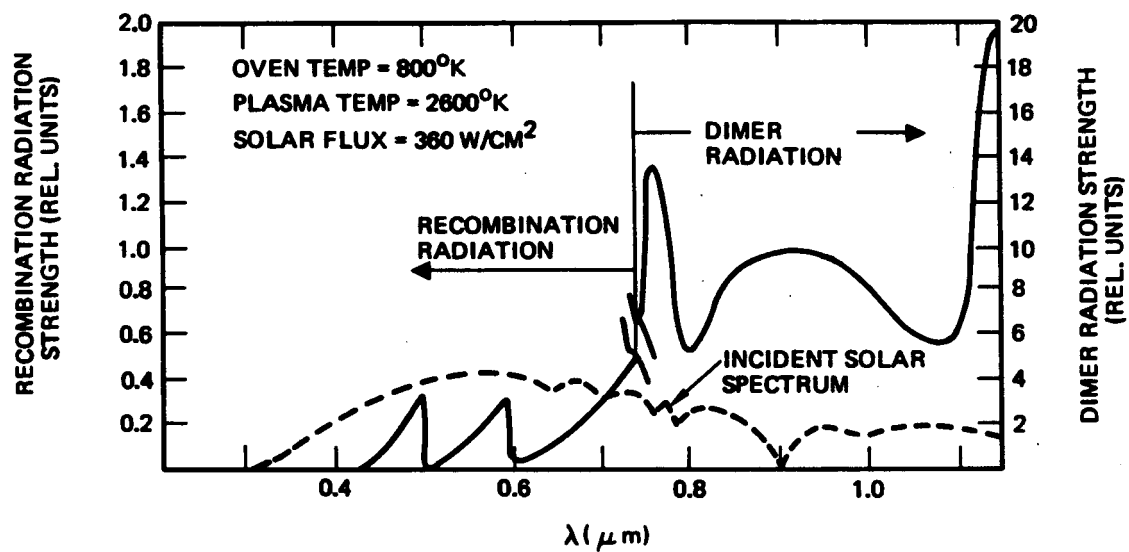


Figure 4. Theoretical solar-sustained plasma re-radiation spectrum (minus line emission).

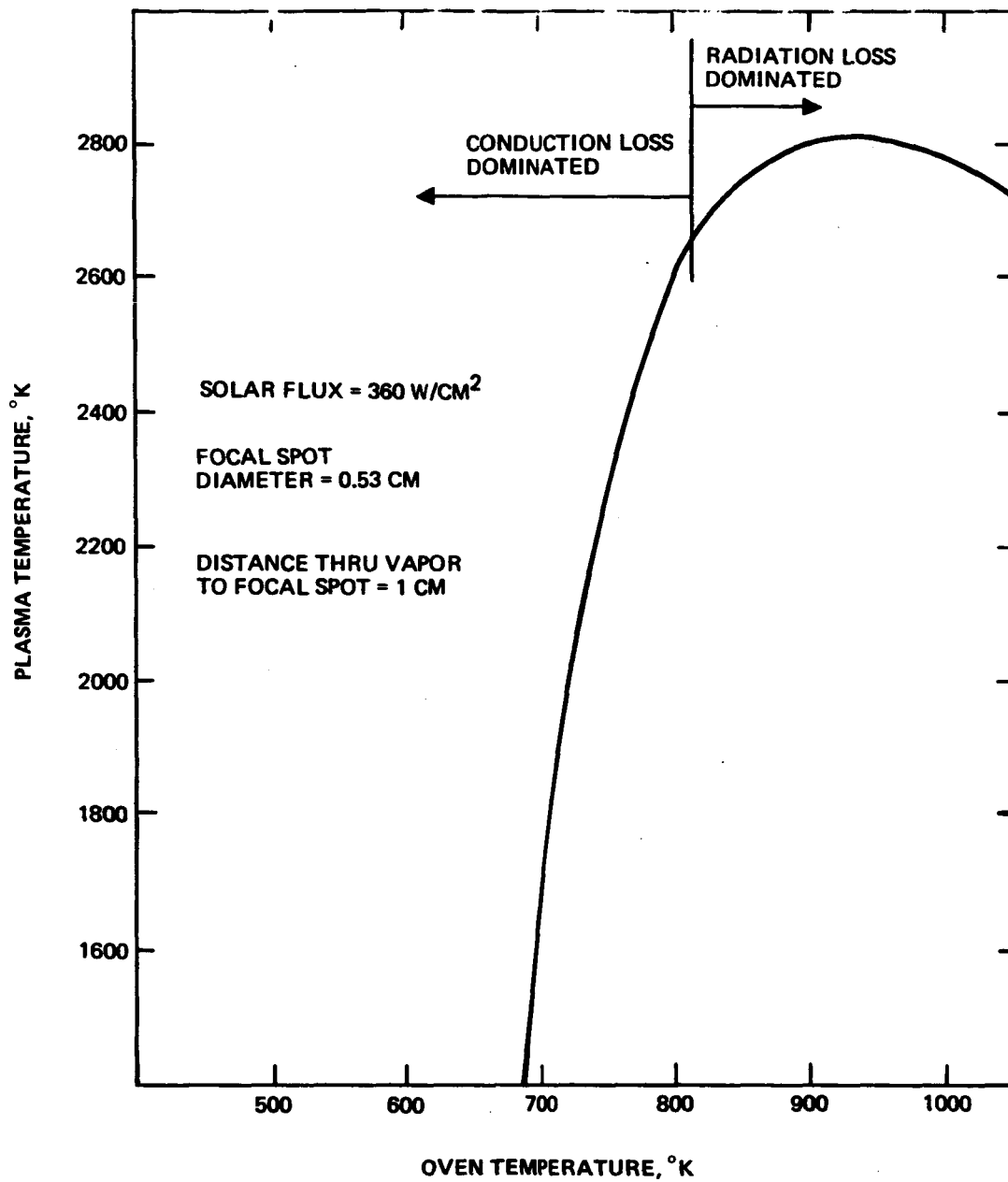


Figure 5. Theoretical plasma temperature as a function of oven temperature showing radiation- and conduction-loss-dominated regimes.

Finally, the model now also accounts for the convergence of the incident radiation and computes the plasma temperature as a function of the propagation distance of the radiation into the vapor. The results, shown in Figure 6, show, for example, that higher plasma temperatures are attainable by positioning the focal volume as close as possible to the front boundary of the vapor.

All of the above plasma maintenance theoretical calculations are done with a computer program written on a time-shared PDP-10 computer. The flow chart and listing for the computer program are presented in Appendix B.

SECTION 3

PLASMA MAINTENANCE - EXPERIMENTAL

Two alternative radiation sources were used on this program. A 1600-W xenon arc lamp adapted with a 10-in.-diameter elliptical reflector for simulating 1000X concentrated sunlight was purchased by HRL as originally planned; it is shown in Figure 7. In addition, a heliostat solar concentrator with a 15-in.-diameter Fresnel lens (shown in Figure 8) that had been used with an earlier solar cell project within HRL was made available for use on this program. This concentrator allowed real sunlight to be used as the radiation source when weather permitted. The oven assembly containing the cesium absorption cell was made portable enough to use with either radiation source.

The first design selected for the cesium absorption cell is shown in Figure 9. This cell was fabricated by ILC Corporation (Sunnyvale, California). It has two 1-in.-diameter sapphire windows (brazed to the cell with an alkali-resistant braze and an internal depleted uranium getter. ILC vacuum baked the cell, loaded it with cesium, and sealed it. They specified the cell to be capable of operating to at least 650°C. This cell design ultimately had to be abandoned because of window failures, but a series of experiments were carried out with the cell in the solar concentrator; these are described below.

The experiments consisted of four basic steps. The first was to measure the spectral intensity of incident sunlight over the continuous range from 3500 to 10,000 Å. The next step was to measure the absorption of the incident sunlight in the vicinity of resonance lines at moderate oven temperature (~150 to 250°C) with the incident sunlight stopped down to less than 1% of the full ~84 W illuminance possible. This was done to confirm that an equilibrium cesium vapor had been obtained in the cell. The third step was to measure the absorption spectra throughout the entire 3500 to 10,000 Å range at an oven temperature of 500 to 600°C. Again, this was done with the incident sunlight stopped way down in

M12755

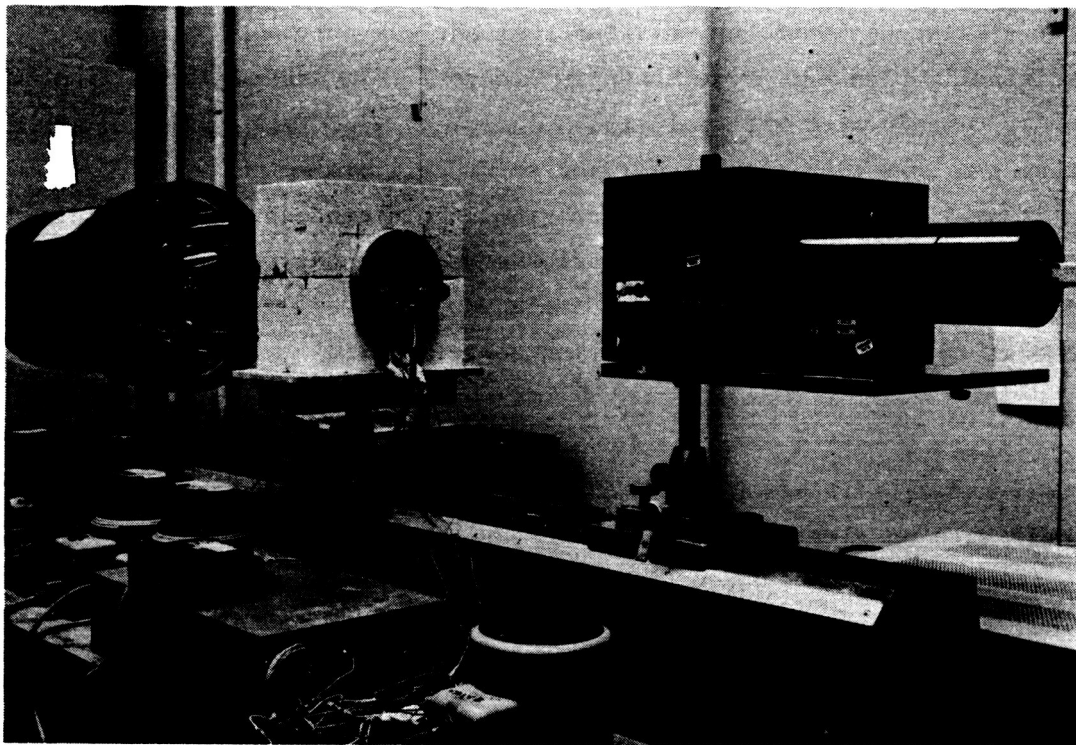


Figure 7. Experimental set-up utilizing arc lamp solar simulator.

M12785

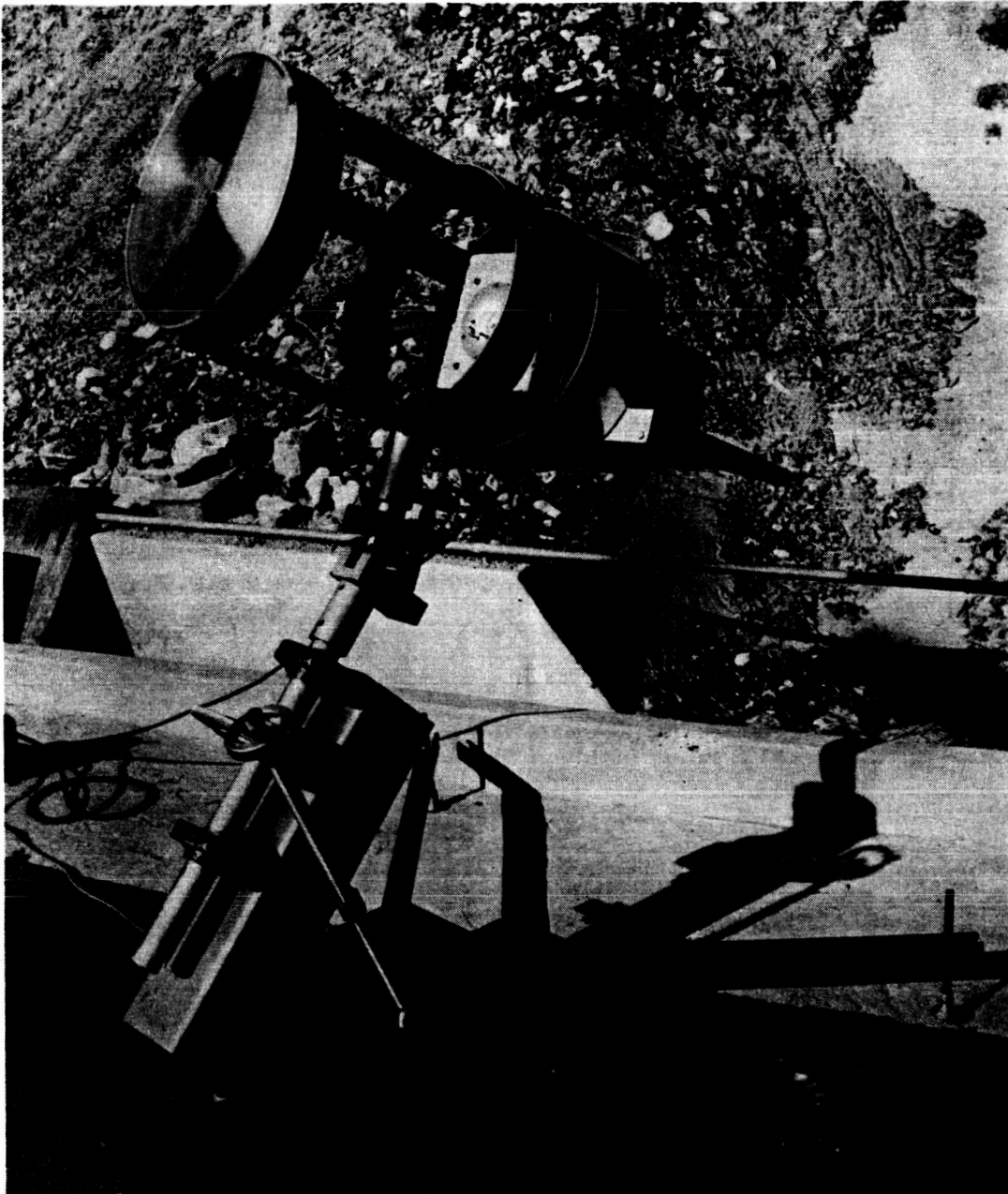
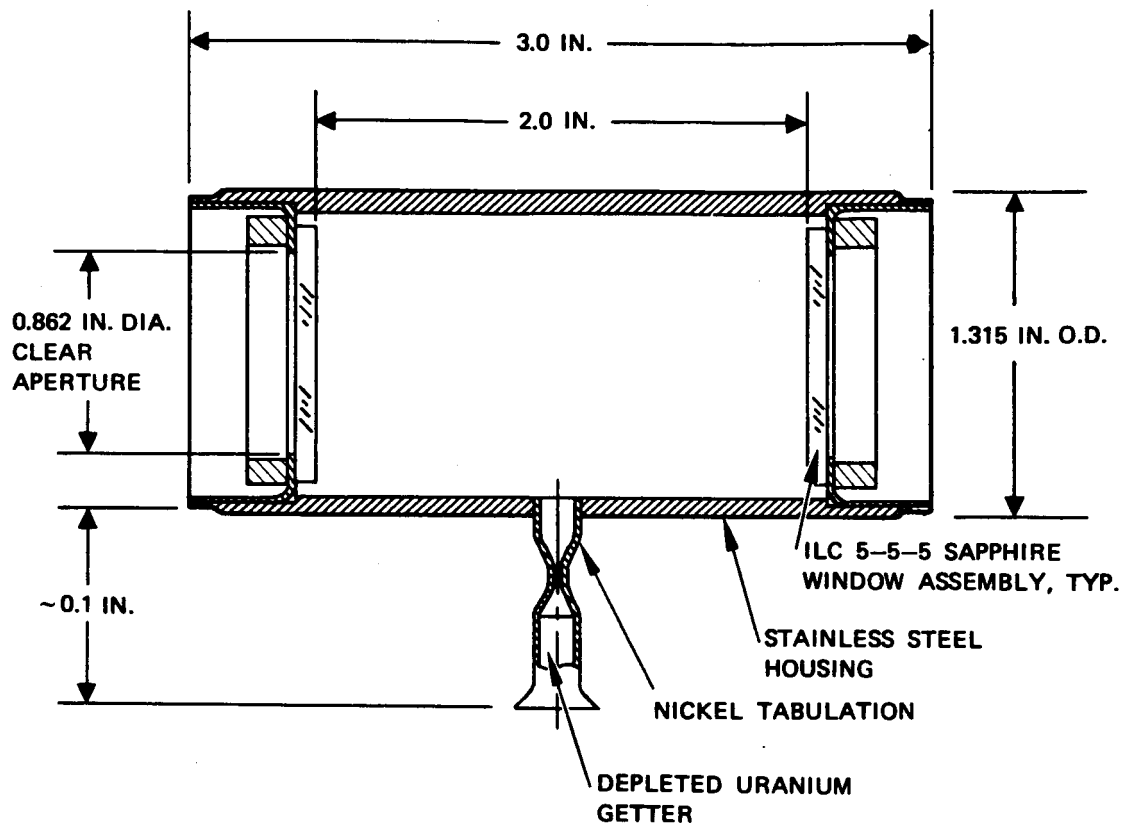


Figure 8. Experimental set-up utilizing solar concentrator heliostat.

**NOTES:**

1. DEVICE VACUUM BAKED AT 600°C
2. FILLED WITH 10 mg CESIUM

Figure 9. Original ILC Corp. cesium absorption cell design.

order to determine the reference absorption spectrum for the cell at these temperatures without a plasma present. The fourth step was to measure the absorption spectra at an oven temperature of 500 to 600°C under full illumination of the ~84 W concentrated solar radiation. The purpose was to ascertain whether a plasma was present by determining if the previously attained absorption spectra had changed.

This first series of measurements yielded the following results:

- Step 1: The incident solar spectra were found to be normal (i.e., complete with the known atmospheric absorption bands).
- Step 2: The absorption strength results at the 8521-Å cesium resonance line are shown in Figure 10 for two different temperatures. Comparing these absorption spectra with the theoretically computed spectra indicates that an equilibrium concentration of cesium vapor had been attained at the temperatures measured.
- Step 3: The absorption spectrum at 500 to 600°C is dominated as expected by the cesium dimer absorption bands. Two of the transmission windows observed at 500°C, one centered at ~4500 Å and the other at 5200 Å, are shown in Figure 11 (a and b) (the two spectra have not been normalized). At 600°C, the only transmission measurable through the cell is in the 5200-Å window.
- Step 4: When the cell was exposed to the full ~84 W of concentrated sunlight, a peculiar dynamics of absorption was observed. The transmitted flux through the cell in the 5200-Å and 4500-Å windows was observed to first increase and then decrease to a value below that of the previous stopped down illuminance measurements in a few seconds (see Figure 11(c and d)). The cause of this was not definitely determined. Although it may indicate that a plasma has been produced, we feel that it more likely is associated with induced condensation of cesium on the windows. Window condensation on a longer time scale was constantly occurring during these measurements, making it virtually impossible to obtain reproducible results.

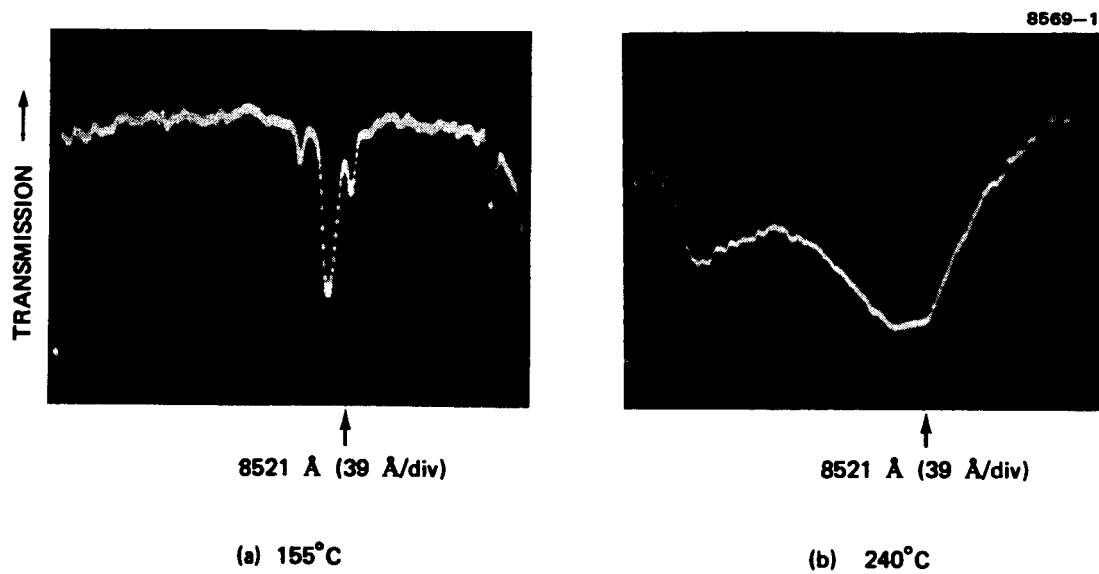


Figure 10. Cesium resonance line absorption.

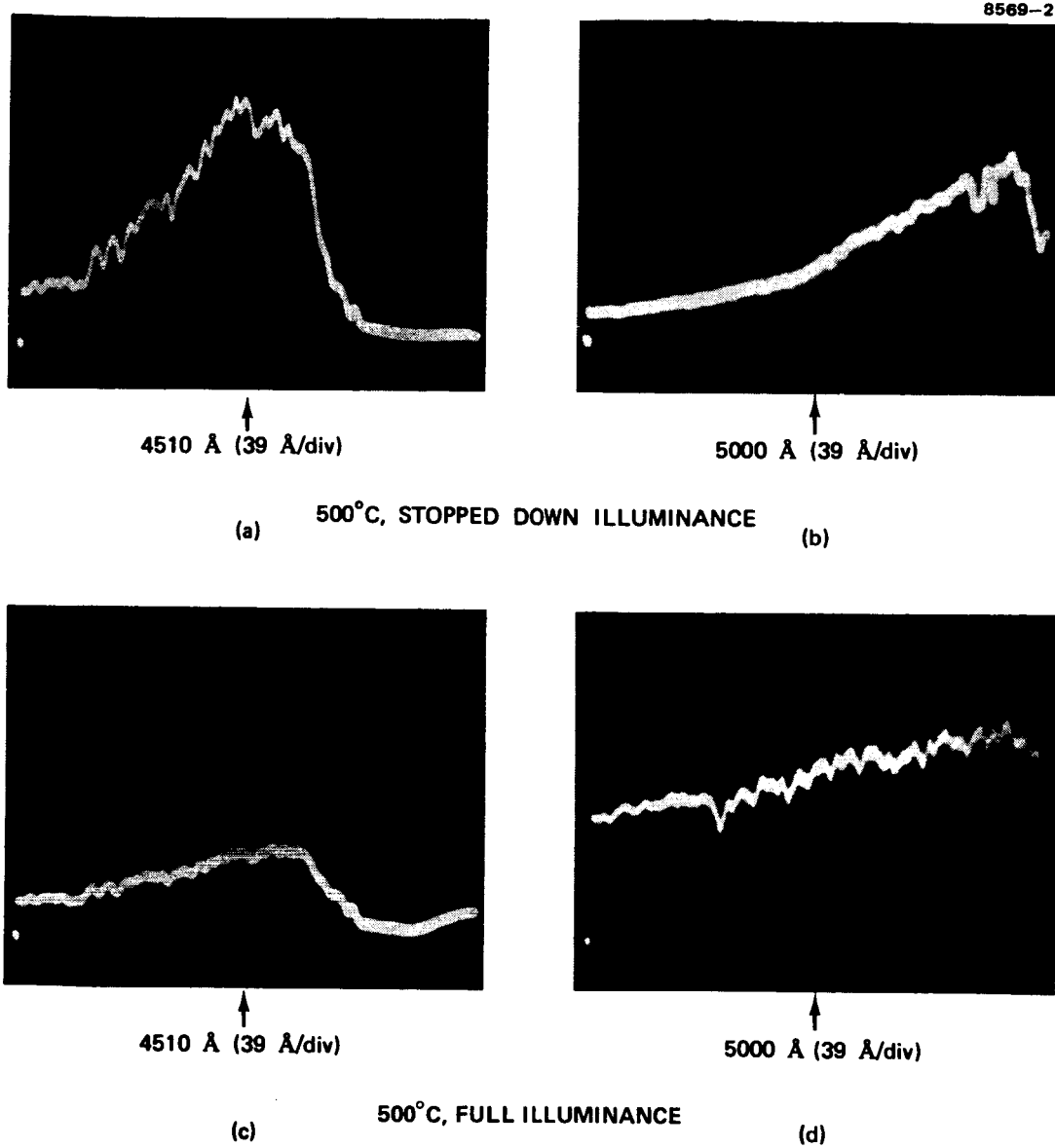


Figure 11. High-temperature cesium absorption spectra under partial illumination from the solar concentrator (a,b) and under full ~ 377 -W illumination from the concentrator (c,d).

Window fogging continued to occur with the above cell design even when high-power window heaters were used. Also, the entrance window on the cell cracked twice, as shown in Figure 12, causing a long delay during repair of the cell at ILC Corporation. After the second window failure, we decided to convert the absorption cell design to that of a heat pipe oven. Heat pipe ovens offer several advantages over equilibrium ovens, such as uniform temperature vapor zones, vapor purification, and isolation of the vapor from the windows.⁷ The latter feature is especially important for our application, not only because it allows using ordinary glass windows and eliminates the window fogging problem, but also because it allows spatial separation of the radiation absorption zone from the region adjacent to the windows. In the previous cell design, it is the conduction of heat to the entrance window from the absorbing vapor adjacent to it that is suspected of causing the window cracking that has occurred with these designs. (Absorption in the sapphire window itself should not have been enough to cause failure.²) Since the vapor pressure in a heat pipe oven is determined by the pressure of the inert gas in the oven,⁷ the cell design included a valve to permit changing the vapor pressure and moving the cell outside when the solar concentrator is used.

The first heat pipe oven design is shown in Figure 13, and a photograph of the fabricated cell installed on the arc lamp optical bench is shown in Figure 14. The first operation of this cell was successfully carried out at an argon pressure of 200 Torr and a central oven temperature of 550°C. Absorption at 8500 Å was monitored during this run, and, although a quantitative reduction of the absorption data was not carried out, the indicated length of the cesium vapor zone appeared to be ~1 cm, as planned. Once again, window fogging precluded further experiments with this cell.

We believe that the window fogging was probably caused by excess cesium lying adjacent to the windows and being heated by the hot argon gas circulating in the end region. The cell was therefore redesigned to

M12908



Figure 12. Cracked entrance window of ILC absorption cell.

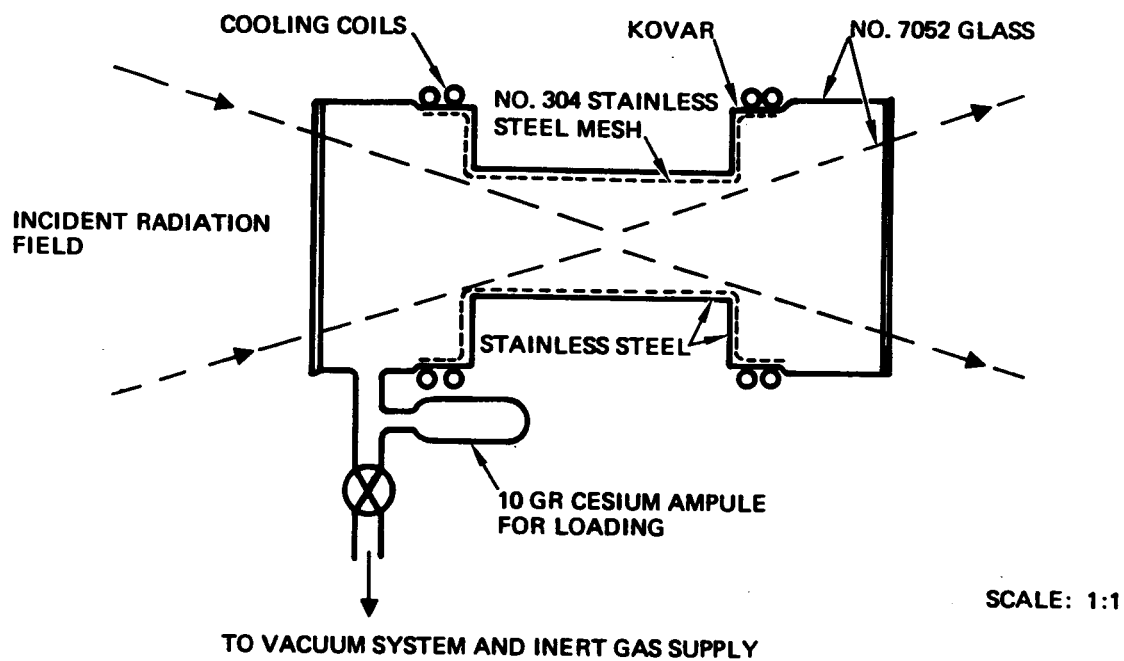


Figure 13. First heat pipe oven design for solar-sustained plasma absorption cell.

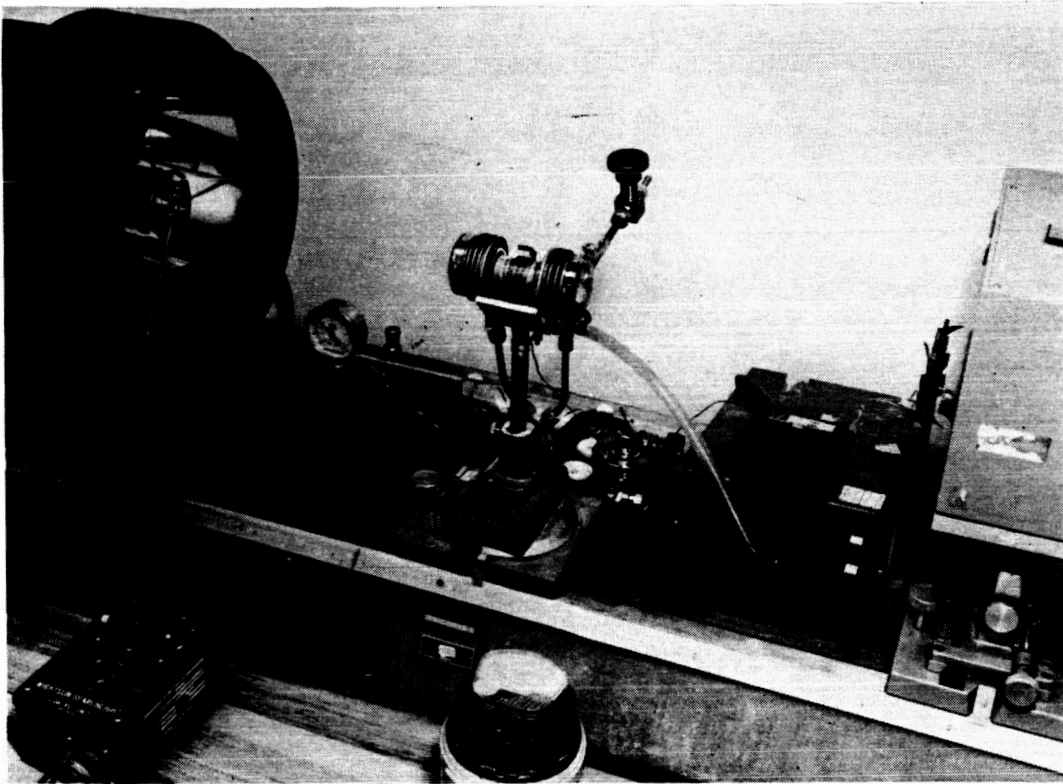


Figure 14. Photograph of first heat pipe oven absorption cell.

put the windows much farther from the heated zone. Figure 15 shows a photograph of this new cell. Since the amount of cesium originally loaded into this cell was insufficient to wet the wick completely, we are currently taking steps to load additional cesium onto the wick.

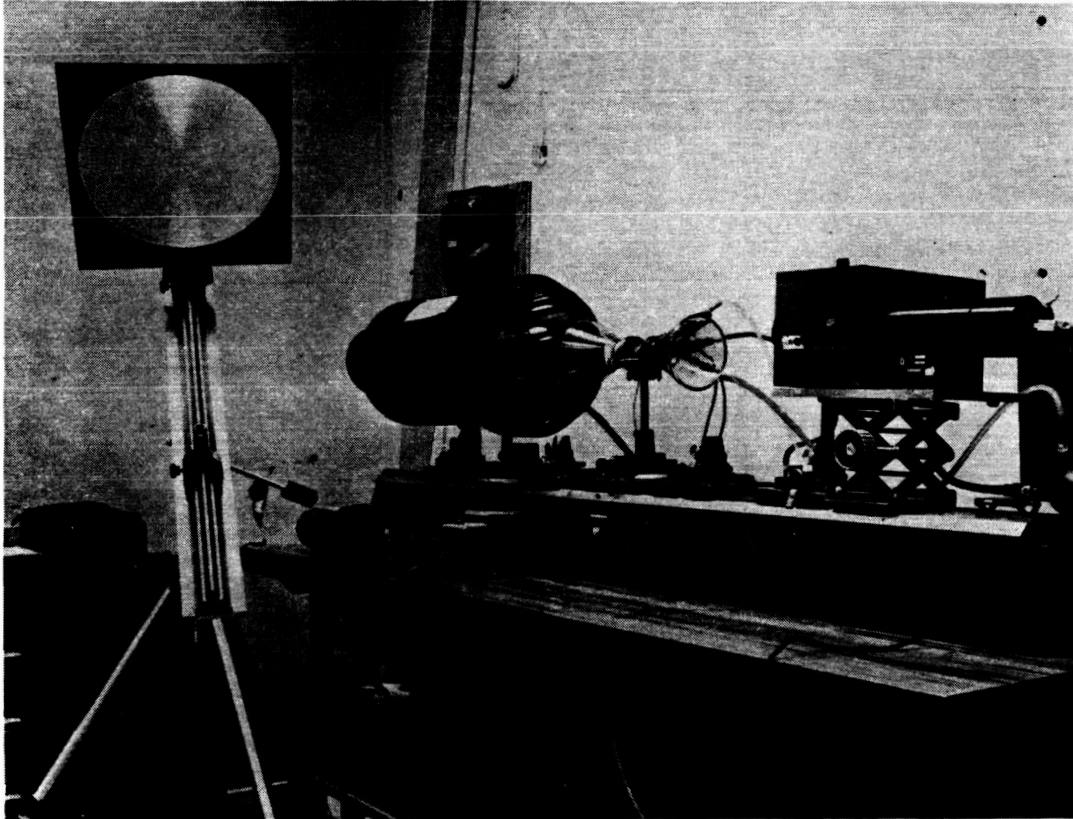


Figure 15. Photograph of latest heat pipe oven absorption cell.

SECTION 4

SOLAR-PUMPED MHD LASER — THEORETICAL

The concept of a solar-pumped MHD laser was first disclosed at the 1978 NASA Ames Conference on Radiation Energy Conversion and in the Hughes Research Laboratories technical proposal for this contract.⁸ It was pointed out then that a population inversion on the cesium dimer A-X laser transition will develop in a solar-sustained cesium plasma if the electron temperature can be made to exceed the gas temperature by at least the fractional red shift of the transition. It was suggested that such a decoupling of the electron and gas temperatures could be made to occur in a nozzle flow of the plasma across a magnetic field. Thus, a closed Rankine cycle solar-pumped laser was identified that is similar in concept to the MHD solar-electric converter with laser power replacing or supplementing electric power as the work output of the cycle. The laser characteristics for this type of transition would include⁹

- High saturation power ($\sim 50 \text{ kW/cm}^2$)
- Large, high-power system capability (low gain, fewer parasitic problems)
- Broadband tunability ($\Delta\lambda \sim 1000 \text{ \AA}$).

During this program, we quantified these speculations with a mathematical model and expanded the lasing transitions considered to include the CsXe A-X excimer band. The excimer laser transition will offer essentially the same advantages as listed above for the dimer transition.⁹ As shown below, the results of the analysis give considerable encouragement to the concept of a solar-pumped high-power MHD laser.

The energy level diagrams showing the CsXe excimer and Cs_2 dimer laser transitions are shown in Figure 16. If the molecular states are assumed to be populated in thermal equilibrium with respect to their parent atomic states at the gas temperature and the population of the atomic states to be in thermal equilibrium at the electron temperature, then the population ratio between the upper and lower molecular levels can be written as

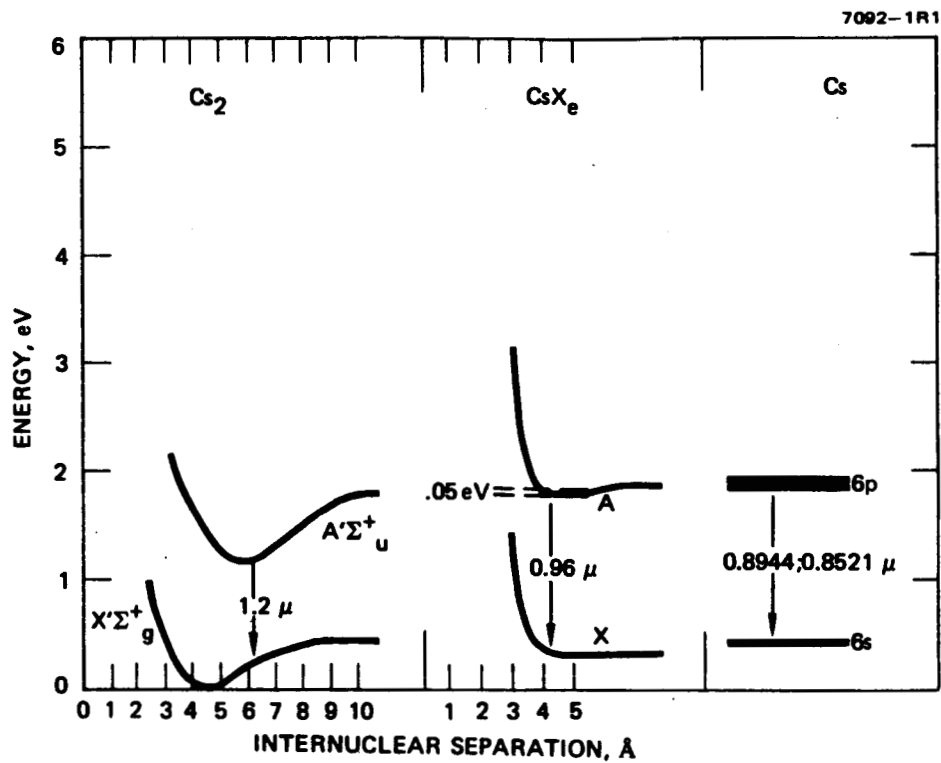


Figure 16. CsXe excimer and Cs_2 dimer laser transitions.

$$\frac{N_u}{N_L} = \frac{g_u}{g_L} \exp \left[\frac{\Delta(h\nu)}{T_g} - \frac{h\nu_o}{T_e} \right], \quad (1)$$

where $\Delta(h\nu)$ is the red shift, $h\nu_o$ is the atomic transition energy, T_g is the gas temperature, T_e is the electron temperature, and g_u and g_L are degeneracy factors. Therefore, an inversion will result under this two-temperature equilibrium condition if the ratio of gas to electron temperature is less than the fractional red shift:

$$\frac{T_g}{T_e} < \frac{\Delta\nu}{\nu_o}. \quad (2)$$

From Figure 16, the fractional red shift is ~ 0.07 for transitions from the bottom of the excimer A state and ~ 0.25 for transitions from the bottom of the dimer A state. Eq. 1 predicts that a population inversion will occur on the excimer band for $T_e/T_g \geq 13$ and on the dimer band for $T_e/T_g \geq 3.9$.

The starting point for calculating the electron and gas temperature in a plasma flow through a Faraday MHD channel (with short-circuited electrodes) is an electron energy balance equation derived by B. Zanderer et al. and utilized in their DARPA-sponsored program to generate 10- μm laser action in an MHD channel:¹⁰

$$(T_e/T_g - 1) = \frac{2}{3} \delta M^2 \gamma \beta_e, \quad (3)$$

where γ is the ratio of specific heats; β is the Hall parameter; M is the Mach number of the flow; and δ is an inelastic collision energy loss factor equal to the ratio of the inelastic electron collisional energy loss rate to the elastic collisional energy loss rate. If a Maxwell-Boltzman energy distribution is assumed for the electron and the excited state population of cesium, then δ may be expressed as:⁹

$$\delta = \frac{(6.38 \times 10^7) (2 T_e)^{3/2} \exp(-E_1/T_e) (1 + E_1/2T_e)}{\sigma_{e1} (2 T_e)^{1/2} (c/m_e^{1/2}) (2m_e/m_{Xe}) (T_e - T_g)} \left. \frac{d\sigma_1}{dE} \right|_{E_1}, \quad (4)$$

where E_1 is the energy of the first excited state of xenon, σ_1 is its excitation cross section, and σ_{e1} is the electron elastic collision cross section.

If we add to Eqs. 3 and 4 the isentropic expansion equation for the gas temperature,

$$T_g/T_o = \left[1 + \frac{1}{2} (\gamma - 1) M^2 \right]^{-1} \quad (5)$$

then we may solve for the electron temperature and gas temperature as a function of the Mach number and the Hall parameter. We assumed $\beta = 3$, $\gamma = 5/3$, $\sigma_{e1} = 3 \times 10^{-15} \text{ cm}^2$, $d\sigma_1/dE|_{E_1} = 3 \times 10^{-17} \text{ cm}^2 \text{ eV}^{-1}$, and $T_o = 3000^\circ\text{K}$. The collisional cross sections σ_{e1} and $d\sigma_1/dE|_{E_1}$ were taken from Ref. 11.

The results for the electron temperature and the ratio of the electron to gas temperature are shown in Figure 17. According to these results, a population inversion on the excimer and dimer transitions will occur for Mach numbers greater than 3 and 0.5, respectively.

The small-signal gain coefficient itself can be computed from the quasi-static theory of line broadening:¹²

$$\text{gain} = \frac{\lambda^2 \tau^{-1}}{8\pi} \left[\frac{d[A]}{dR} - \frac{g_A}{g_X} \frac{d[X]}{dR} \right] \frac{dR}{dv}, \quad (6)$$

where λ and τ are, respectively, the wavelength and radiative lifetime of the transition; ν is the frequency of the transition at the inter-nuclear separation R ; $[A]$ and $[X]$ symbolize the concentrations of the A state and X state, respectively; and g_A and g_X are their degeneracies. In the strongly inverted regime, this gain can be written

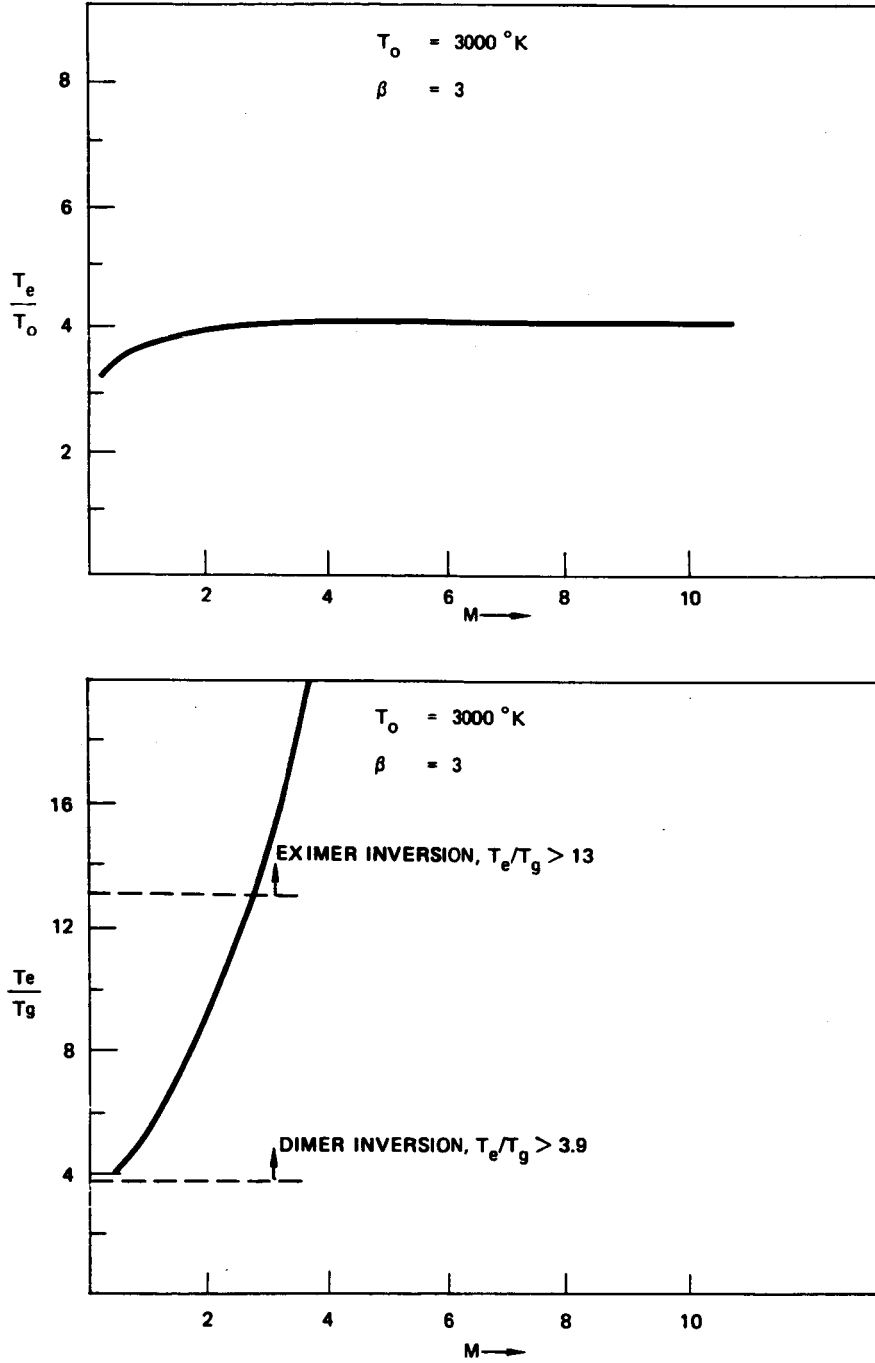


Figure 17. Theoretical electron and gas temperature versus Mach number for solar-sustained plasma flow across a magnetic field.

$$\text{gain}(\lambda) = \alpha(\lambda) [A] \frac{\exp(-V(\lambda)/T_g)}{K_A (g_f/g_A)} , \quad (7)$$

where K_A is the A state equilibrium constant, g_f is the degeneracy of the A state atomic parent state, $V(\lambda)$ is the potential energy of the A state at the internuclear separation corresponding to the transition wavelength λ , and $\alpha(\lambda)$ is the stimulated emission coefficient given by

$$\alpha(\lambda) = \left(\frac{1}{2\pi c} \right) R^2 \frac{dR}{d\nu} . \quad (8)$$

At the temperatures and densities of interest here, the population of the CsXe A state is controlled by the heavy particle dissociation rate. In this case, the A state population will be in equilibrium with its parent atomic state, and Eq. 7 reduces to

$$\text{gain}_{\text{ex}}(\lambda) = \alpha(\lambda) \exp(-V(\lambda)/T_g) [\text{Cs}^*][\text{Xe}] , \quad (9)$$

where $[\text{Cs}^*]$ represents the concentration of cesium atoms in the 6P resonance state.

On the other hand, the Cs_2 A state population will not be in thermal equilibrium with the parent atomic state at the temperatures and densities of interest. This is because its relatively large dissociation energy will cause the collisional dissociation rate of this state to be far below the radiative rate. With the radiative rate dominating the loss of the dimer A state, Eq. 7 for the gain coefficient becomes

$$\text{gain}_{\text{di}}(\lambda) = \alpha(\lambda) \Gamma [\text{Cs}^*][\text{Cs}][\text{Xe}] \tau \left(\frac{\exp(-V(\lambda)/T_g)}{K_A} \right) , \quad (10)$$

where Γ is the three-body association rate coefficient for the formation of the A state. The maximum gain coefficient on the excimer and dimer bands occurs at 0.96 μm and 1.2 μm , respectively. The scaling arguments presented in Ref. 13 lead to $\Gamma \approx 1 \times 10^{-31} \text{ cm}^6 \text{ sec}^{-1}$ and $K_A \approx 8 \times 10^{-23} \exp(-V_A/T_g)$, where V_A is the potential energy at the bottom of the dimer

A state well. Using these numerical values in Eqs. 8 through 10, we find approximately that

$$\text{gain}_{\text{ex}}(0.96 \mu\text{m}) = 7.8 \times 10^{-38} \exp(0.05/T_g) \exp(-1.45/T_e) [\text{Cs}][\text{Xe}] \quad (11)$$

$$\text{gain}_{\text{di}}(1.2 \mu\text{m}) = 1.3 \times 10^{-54} \exp(-1.45/T_e) [\text{Cs}]^2 [\text{Xe}] \quad (12)$$

We have assumed that the population of the 6P resonance level at 1.45 eV is in equilibrium with the ground state at the electron temperature. All temperatures are in eV, concentrations are in cm^{-3} , and the gain coefficients are in cm^{-1} .

The stagnation cesium density for the plasma flow was chosen to be compatible with the efficient coupling of solar radiation to the plasma through dimensional scales on the order of several centimeters, while the xenon density was limited by the upper limit to practical magnetic field strength (~ 40 kG) to yield the assumed value of 3 for the Hall parameter. The chosen stagnation densities were:

$$[\text{Cs}]_0 = 3 \times 10^{18} \text{ cm}^{-3} \quad (13)$$

$$[\text{Xe}]_0 = 3 \times 10^{19} \text{ cm}^{-3} \quad (14)$$

At an assumed temperature of 3000°K for the solar-heated plasma, these densities correspond to a stagnation pressure of ~ 10 atm.

The small-signal gain coefficients on the dimer and excimer bands were computed for these conditions as a function of Mach number using Eqs. 3 through 5 and Eqs. 11 and 12; the results are shown in Figure 18. The figure also shows the magnetic field required to maintain the assumed value of 3 for the Hall parameter. The magnetic field is given by:

$$B = (0.55 \times 10^{-18}) [X_e](\beta) \quad (15)$$

where B is in kG.

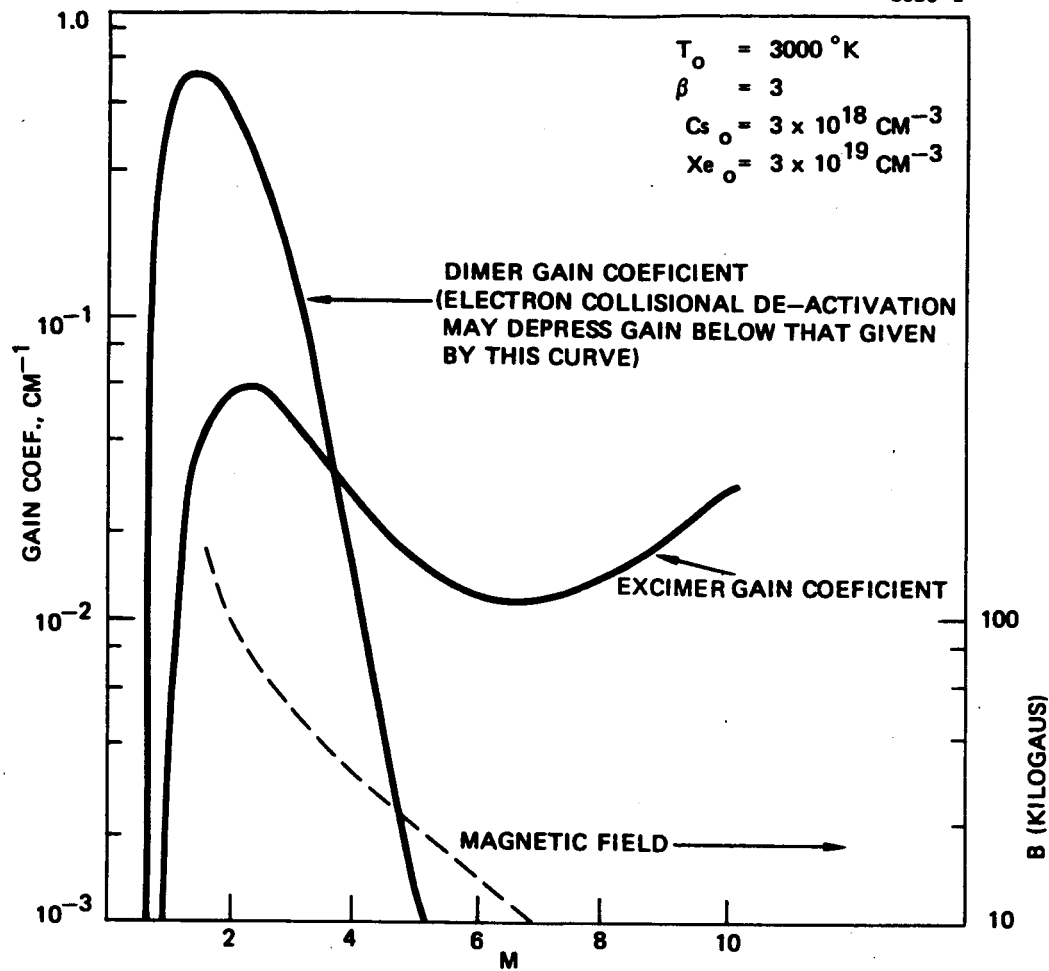


Figure 18. Theoretical gain coefficients and required magnetic field strength for solar-sustained plasma flow across a magnetic field.

The results shown in Figure 18 indicate that gain coefficients large enough to construct a laser are obtainable on both the dimer and excimer bands under quite practical regimes of flow parameters and magnetic field.

As indicated in Figure 18, electron collisional de-excitation and dissociation may depress the dimer gain. This was the case in the modeling of previous static-discharge-pumped alkali systems.^{18,14} An accurate assessment of the influence of electron collisional deactivation of the dimer A state must await a more complete numerical model since it depends sensitively on dissociative recombination rates and multi-step ionization rates. Electron deactivation is not expected to affect the excimer gain because of the high heavy particle dissociation rate controlling the population of the excimer A state.

An important and fortuitous circumstance also occurs for the set of flow parameters chosen. The three-body association rate coefficient for the formation of A-state CsXe excimers and Cs₂ dimers ($\sim 10^{-31} \text{ cm}^6 \text{ sec}^{-1}$) is known to be roughly an order of magnitude larger than the corresponding rate coefficient for the ground-state Cs₂ dimers ($10^{-32} \text{ cm}^6 \text{ sec}^{-1}$).¹³ For a Mach 4 flow speed at the assumed stagnation densities, the recombination times for the Cs-Xe A state, the Cs₂ A state, and the Cs₂ X state will be $\sim 10^{-5} \text{ sec}$, $\sim 10^{-4} \text{ sec}$, and $\sim 10^{-3} \text{ sec}$, respectively. These correspond to distances in the flow of $\sim 0.3 \text{ cm}$, $\sim 3 \text{ cm}$, and $\sim 30 \text{ cm}$, respectively. Thus, a zone in the flow direction of about several centimeters in length will exist in the flow where equilibrium populations have been established on the upper laser levels (as assumed in the above model) but where the population of the ground-state dimers is still frozen at the much lower value determined by the stagnation temperature and the expansion. The absorption cross section at the $0.96\text{-}\mu\text{m}$ excimer band due to ground-state dimers is $\sim 4 \times 10^{-16} \text{ cm}^2$. Normally this dimer absorption would prohibit a net excimer gain from being realized above a cesium monomer density of $\sim 10^{16} \text{ cm}^{-3}$. This upper limit on the alkali density was at the root of failures in past programs to achieve alkali-rare gas excimer laser action utilizing static discharges.^{19,15} In our case, the absorption due to dimers is less than 1/10 of the excimer gain with cesium monomer concentration at $\sim 3 \times 10^{17} \text{ cm}^{-3}$. This justifies using Eq. 11 for the excimer gain.

SECTION 5

FUTURE WORK

During the next 12-month period on this program, first priority will be given to the experimental demonstration of ignition and the maintenance of a cesium plasma by concentrated sunlight. The newly designed heat pipe oven absorption cell will be used for this purpose. The radiation source utilized will include both the arc lamp solar simulator and the 15-in.-diameter Fresnel lens solar concentrator. Once ignition and maintenance of the plasma have been demonstrated visually and photographically, emission and absorption spectral measurements will be made on the plasma and compared with the newly upgraded theoretical model to help provide a complete physical characterization of the plasma. Further experimentation with the plasma during this period will be devoted to scaling studies of the plasma under a factor of two increase in the input solar flux using a larger Fresnel lens.

A large portion of the theoretical effort during the next year will be applied to the construction of a complete numerical model of the MHD nozzle flow of a solar-sustained cesium-xenon plasma for the purpose of predicting the efficiencies of conversion of plasma enthalpy to laser power and electric power, and of predicting associated optimization conditions.

REFERENCES

1. A.J. Palmer, Prog. in Astronautics and Aeronautics 61, 201 (1979).
2. A. Hertzberg, R. Dehker, A.T. Mattich, and C.R. Lau, paper No. 78-1177, AIAA 11th Fluid and Plasma Dynamics Conference, Seattle, Wash., July 10-12, 1979.
3. R. Rodgers, N. Krascella, and J. Kendall, "Solar Sustained Plasma," Final Technical Report, Contract NAS 2-10010, February 1979.
4. A.E. Wechsler, "Characteristics of Metal Vapor," Arthur D. Little Inc., Cambridge, MA, Aerospace Research Laboratories Report ARL 66-004, January 1966.
5. American Institute of Physics Handbook, McGraw-Hill, 1963.
6. W. Vincenti and C. Kruger, Introduction to Physical Gas Dynamics, John Wiley & Sons, New York, 1965.
7. C.K. Vidal and J. Cooper, J. Appl. Phys. 40, 3370 (1969).
8. "Radiatively Sustained Cesium Plasmas for Solar Energy Conversion," Hughes Research Laboratories Technical Proposal No. 78M-0201/E2692, February 1978.
9. A.J. Palmer, L.D. Hess, et al., "Excimer Lasers," Final Report, NASA Contract NAS 3-19707, November 1977.
10. B. Zanderer, et al., "CO₂MHD Laser; Analysis, Design and Shock Tunnel Experiments," Proc. 14th Symposium on Engineering Aspect of MHD (1974).
11. L.J. Kieffer, Jr. Inst. Lab. Astrophys. Information Center Rpt. No. 13, University of Colorado, September 30, 1973.
12. A.J. Palmer, J. Appl. Phys. 47, 3088 (1976).
13. C. York and A. Gallagher, Jr. Inst. Lab. Astrophys. Report 114, October 1974.
14. A.C. Gallagher and A.V. Phelps, Final Technical Report, ERDA Contract No. E(49-1)-3800, February 1977.
15. H. Rothwell, D. Leep, and A. Gallagher, J. Appl. Phys. 49 (1978).

APPENDIX A

Radiatively Sustained Cesium Plasmas for Solar Electric Conversion

A. Jay Palmer

Reprinted from Radiation Energy Conversion in Space, edited by Kenneth W. Billman, Vol. 61 of Progress in Astronautics and Aeronautics.

RADIATIVELY SUSTAINED CESIUM PLASMAS FOR SOLAR ELECTRIC CONVERSION

A. Jay Palmer*

Hughes Research Laboratories, Malibu, Calif.

ABSTRACT

We discuss a new concept for solar electric conversion based on the maintenance of an optical discharge in cesium vapor by concentrated solar radiation. The radiation is absorbed on excited state photoionization transitions and dimer transitions and electric power is coupled out of the plasma via MHD. The results of a computer model of the radiatively maintained discharge predict that an optical discharge can be maintained at a plasma temperature of 3000 to 3500°C by solar radiation concentrated by a factor of a few thousand incident on cesium vapor at a vapor pressure of one atmosphere. The conductivity of the plasma is $\sim 10^3$ mho/m which is comparable to the plasma conductivity in existing MHD generators.

INTRODUCTION

In the heat engine approach to solar-electric conversion, it is advantageous for achieving highest efficiency to deposit the radiation directly into the working fluid at the maximum possible temperature. If this temperature is to approach anywhere near the upper limit of the sun's temperature, then the working fluid will necessarily be a plasma and electric power must be coupled directly out of the plasma directly utilizing, for example, MHD. It is of interest therefore to identify a plasma in the temperature range of 3000 to 6000°K which can present a broadband absorption cross section throughout the solar spectrum which is large enough to permit the use of moderate densities and dimensional scales for efficient coupling of the radiation to the plasma.

Broadband absorption of visible radiation in plasmas can occur from primarily two causes: Inverse-bremsstrahlung (free-free electron transitions) and photoionization (bound-free electron transitions). If one assumes thermal ionization described by Saha's equation, then the absorption cross section (per ground state) due to free-free transitions in a hydrogen-like plasma is (Ref. 1)

$$\sigma_{ff} = 7.9 \cdot 10^{-18} \left(\frac{V_I}{h\nu} \right)^3 \frac{\exp(-V_I/T)}{2 \cdot (V_I/T)} \text{ cm}^2 \quad (1)$$

where V_I , T and $h\nu$ are the ionization potential, the plasma temperature and photon energy respectively. At a temperature near 5000°K one sees that even with a low ionization potential species, the cross section is quite small so that very high densities with associated formidable plasma pressures will be required to yield a practical value for the free-free absorption coefficient in the solar spectrum ($h\nu \sim 1-3$ eV).

*Member of Technical Staff.

On the other hand the absorption cross section due to bound-free transition can be much larger in the visible than the free-free cross section. Combining Kramer's formula for the hydrogenic bound-free cross section per excited state with an assumed Boltzmann distribution for the excited state population gives the cross section per ground state as, (Ref. 1)

$$\sigma_{bf} = 7.9 \cdot 10^{-18} \left(\frac{v_I}{h\nu} \right) \sum_{l=1}^{\infty} \frac{(2L(i) + 1)}{n^*(i)^3} \cdot \exp \left(-\frac{E(i) - v_I}{T} \right) \quad (2)$$

where $n^*(i)$, $L(i)$ and $E(i)$ are the effective principle quantum number, the total angular momentum quantum number, and the binding energy respectively of the i^{th} excited state.

For the temperatures of interest (3000 to 5000°K) cesium will exhibit the largest average bound-free cross section throughout the solar spectrum. In addition cesium has other important continuum absorption bands in the red portion of the solar spectrum due to ground state cesium dimers. These absorption bands extend from about 6000 Å to 1 micron which, conveniently, is where the bound-free cross section is falling off. The dimer absorption cross section may be computed from the quasi static theory of line broadening (Ref. 2). This technique requires knowledge of the potential energy curves for the transition and partitions the molecular states into a set of substates characterized by their internuclear separation and populated relative to their dissociation products according to a classical canonical ensemble. Thus the concentration of dimers in the ground electronic state with an internuclear separation between R and $R + dR$ is written as (Ref. 3)

$$d[X] = 4\pi R^2 dR (g_x/g_{x,f}) \exp(-WX(R)/kT) [Cs]^2. \quad (3)$$

Here $[]$ indicates species concentration, g_x and g_f are the degeneracies of the molecular X state and its parent atomic state respectively. $WX(R)$ is the energy of the molecular substate relative to that of its parent atomic state, k is Boltzmann's constant, and T is the gas temperature.

The absorption coefficient due to a ground state dimer transition can, therefore, be written immediately as (Refs. 2 and 3)

$$\beta = \frac{\lambda^2}{2} \frac{A \cdot R^2}{d\nu/dR} \exp \left(-\frac{WX(R)}{kT} \right) \frac{g_x}{g_{x,f}} [Cs]^2. \quad (4)$$

where A is the Einstein coefficient for the transition (assumed independent of R), and λ and ν are the wavelength and frequency of the radiation.

The absorption cross section for the cesium dimer $X \leftrightarrow A$ transition and a hypothetical $X \leftrightarrow B$ transition were computed in this way. The dimer potential energy curves were approximated as Morse potentials. The A and X state were specified with dissociation energies taken from Hertzberg (Ref. 4) and internuclear separations at the potential minima chosen to best match the spectra observed in reference (5). The hypothetical B state was a shallow Morse potential with an internuclear separation at potential minimum set equal to that of the ground state and a well depth chosen to reproduce an absorption band whose width corresponds approximately with the overall width of the set of overlapping $X-B$, $X-C$, $X-D$, etc. absorption bands observed in Cs in the spectral range between roughly 7500 Å to 6000 Å (Ref. 6). (The broadband nature of the incident radiation and the assumption of LTE combine to make the results of the forthcoming energy balance calculation relatively insensitive to the exact shape of the $X-B$ absorption band.)

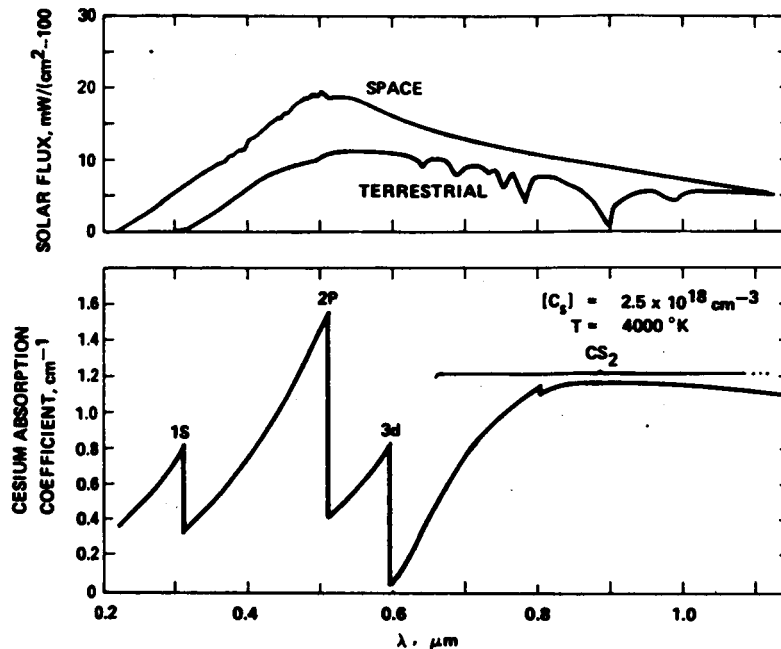


Fig. 1 Solar spectrum and cesium absorption spectrum.

The net absorption coefficient due to both the bound-free transitions and the dimer transition in an LTE cesium plasma at a computed temperature of 4000°K and a pressure of ~ 2 atm. is shown in Figure 1, from Eqs. (2) and (4) where it is compared with the solar spectrum. Both the spectral profile and the magnitude of the cross section are seen to be well suited for the use of cesium at moderate densities as an efficient solar radiation receiver. These features together with its relatively high vapor pressure at practical operating temperatures, its high electrical conductivity and its availability seem to uniquely identify cesium as an optimal working fluid for an advanced, high temperature solar-electric heat engine.

THEORETICAL MODEL FOR A SOLAR SUSTAINED CESIUM PLASMA

In this section we first present an approximate model which can be used to predict the cesium plasma temperature that a given solar flux can sustain against radiative losses alone in an assumed homogeneous static plasma. This model serves to illustrate the limitations to achieving higher temperatures which are imposed by radiation losses alone. Subsequently we expand the model to include gas flow as would occur, for example, in the working fluid of a solar electric heat engine.

The basic assumptions of the model are that local thermodynamic equilibrium obtains and that the electron and heavy particle temperature are equal. At the cesium vapor densities of interest ($\sim 10^{19}$ cm $^{-3}$) electron-heavy particle collisional energy transfer rates will dominate over radiative and other convective energy transfer rates making these assumptions valid.

STATIC CASE

In the static plasma model the plasma temperature was assumed independent of position in the plasma and was computed by merely balancing the energy

absorbed on the two dimer transitions and photoionization transitions from the first eight excited states of cesium against energy lost to radiative recombination into these same states and the dimer spontaneous emission rates. The radiative rates were calculated on the basis of detailed balancing applied to the absorption cross sections. Rates into and out of states higher than the eighth excited state of cesium were verified to contribute negligibly to the overall energy balance in the plasma.

The energy balance calculations were carried out with the aid of a computer program. The results of the computer calculations are shown in Figure 2 as a plot of the required solar flux in Watts/cm² for maintaining a cesium plasma against radiative losses versus the attainable plasma temperature. The solar spectrum was taken as the spectrum of a black body at a temperature of 5800°K. The concentration ratio required to achieve these fluxes for a 1 kW/m² solar flux assumed incident at the earth is shown on the right-hand ordinate. The maintenance flux for a perfect black body is shown for comparison. One sees that with the use of 10³ power concentrations, one can achieve plasma temperature of ~3500°K. For this result to be valid for the static plasma it is necessary that the energy loss to thermal conduction be small compared with radiative losses and that the spatial extent of the plasma along the radiation propagation direction be small compared with the smallest penetration depth of the solar spectrum in the plasma. These conditions will be approximately satisfied for a 1 cm diameter spherical cesium plasma at the assumed density for the temperature range between ~2500 to 4000°K.

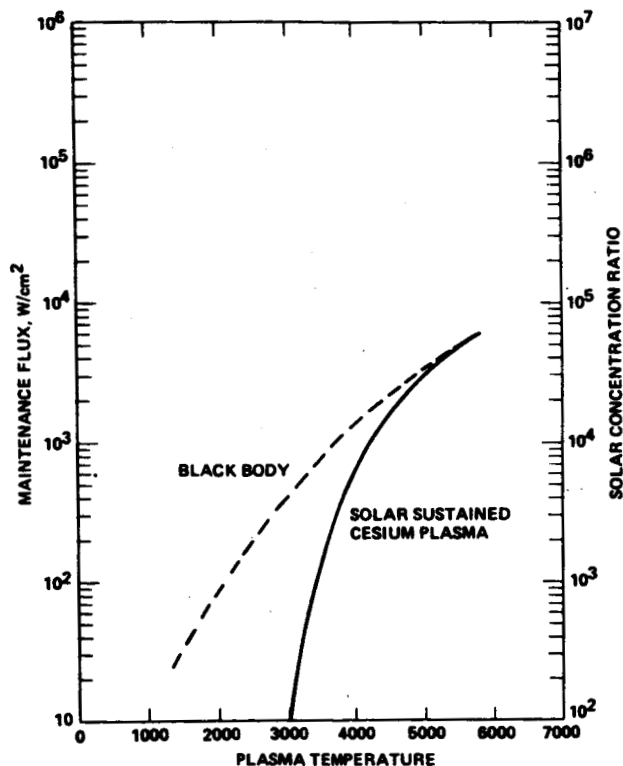


Fig. 2 Solar flux required for sustaining a cesium plasma against radiation losses only.

It is possible to understand the general form of the result presented in Figure 2 on the basis of a simple physical argument based on the principle of detailed balancing. The argument goes as follows.

Consider a system which is absorbing and emitting radiation on one transition only. If the system is in steady state, then the energy balance condition reads:

$$P(\nu) \cdot \sigma \cdot (n_l - n_u) = n_u \cdot A \cdot (h\nu) \quad (5)$$

where n_u and n_l are the population densities of the upper and lower level for the transition, σ is the absorption cross section for the transition. A is the spontaneous radiative rate and $P(\nu)$ is the input radiative power flux to the system at the transition wavelength. Now, if the level populations are in thermal equilibrium at a temperature T , then from detailed balancing $P(\nu)$ is the Plank spectrum:

$$P_T(\nu) = \frac{2h\nu^3}{c^2} (e^{\frac{h\nu}{kT}} - 1)^{-1} \quad (6)$$

Alternatively, if black-body radiation from a radiator of temperature T_R is to sustain the system at a temperature T , then the energy balance condition reads

$$C P_{T_R}(\nu) = \frac{A(\nu) \frac{n_u}{n_l}}{\sigma} \Big|_T = P_T(\nu) \quad (7)$$

where C is a factor which is equal to one at the surface of the radiator. Obviously $C = 1$ for $T = T_R$. If $T_R \neq T$, then

$$C = \frac{P_T(\nu)}{P_{T_R}(\nu)} \quad (8)$$

From the form of the black-body spectrum (Eq. 6) $C < 1$ for $T < T_R$ and $C > 1$ (optically impossible) for $T > T_R$.

The above argument continues to hold (term by term) for a system absorbing black-body radiation on more than one transition and, in particular, on the continuum bound-free and dimer transitions. The essential condition for the validity of the argument is that the system energy balance be dominated by radiation, that the input radiation be in a black-body spectrum, and that the system be in thermal equilibrium at some temperature, $T < T_R$.

In the case of several transitions or continuum transitions the value for C will be determined from a spectrum integration of Eq. (8) and this is what is done in the computer program to obtain the solid curve in Figure 2. For an estimate one can characterize the system with some average wavelength in the absorption spectrum weighted by the input radiation spectrum. In our case this wavelength is near 5000 Å. In this case

$$C = (\exp(\frac{h\nu}{T}) - 1)^{-1} / (\exp(\frac{h\nu}{T_R}) - 1)^{-1} \approx \exp(-\frac{2}{T} - \frac{2}{.58}) \quad (9)$$

and this is the general form of the solid curve given in Figure 2.

The same arguments can be applied to line transitions in the plasma. But, since in the bulk of a plasma which has been made to have an optical thickness of ~ 1 for the bound-free transitions, the line transitions contribute negligibly to the energy flux and they can be neglected altogether.

CONVECTIVE CASE

The static case analysis above serves to identify the minimum input power required to maintain the plasma at a given temperature against radiative losses only. Such a static radiatively maintained plasma will not obtain in practice especially if the plasma is to assume the role of a heat engine working fluid where the plasma must necessarily dissipate a significant fraction of its thermal energy non radiatively in performing work. In particular, at 3000°K the only mechanism for coupling electric power out of the plasma at a rate which can compete with the radiative energy loss rate of the plasma appears to be MID.

We therefore adopt a one-dimensional convection model of a radiatively sustained plasma similar to that used by Raizer (Ref. 7) for laser sustained plasmas where the plasma temperature is allowed to depend on position along the propagation direction and the gas flow is assumed to occur at constant

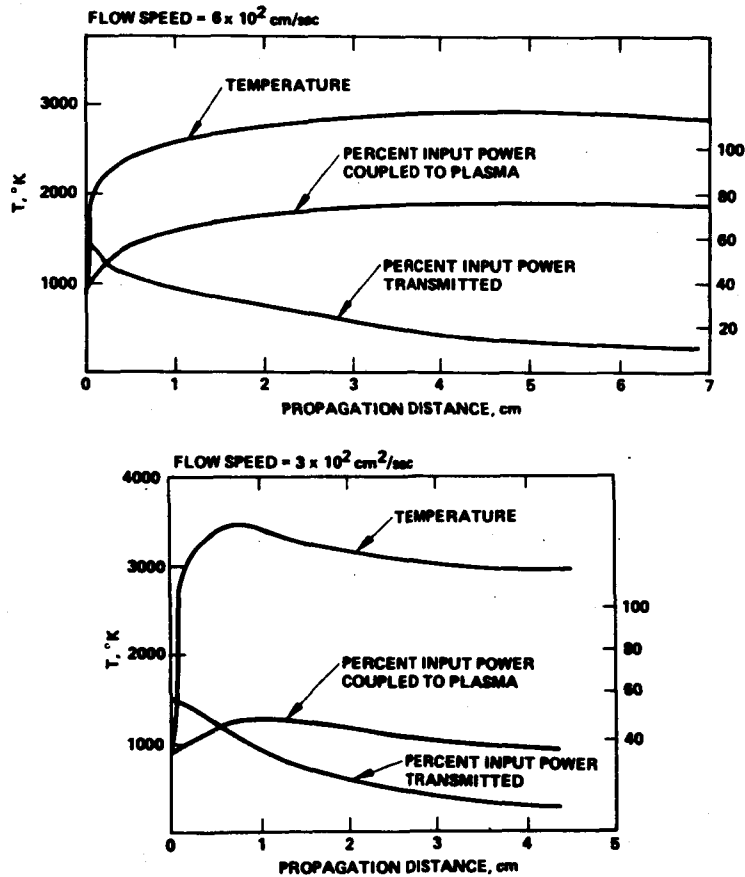


Fig. 3 Plasma temperature, coupling efficiency and transmission coefficient as a function of propagation distance in a cesium plasma from the one-dimensional convective model (oven temperature = 1000°C, solar concentration ratio = 3000).

pressure. The energy balance condition then reads

$$\frac{3}{2} N_0 U C_p \frac{dT}{dz} = W(z) - R(z) + \frac{d}{dz} \left(K \frac{dT}{dz} \right) \quad (10)$$

where N_0 and U are the gas density and flow velocity at the point where the gas enters the interaction zone, C_p is the specific heat, K is the thermal conductivity, $W(z)$ and $R(z)$ are the radiative energy deposition and radiative loss respectively per unit volume, T is the gas temperature, and z is the distance along the propagation direction of the incident radiation.

We may once again neglect the energy loss due to thermal conduction. This is because, under the conditions we consider, the radiation penetration depths and convective energy transfer rates combine to yield relatively gradual temperature gradients. This is in contrast to the laser sustained plasma modeled by Raizer (Ref. 7) where thermal conduction is in fact responsible for maintaining the discharge. There the cold gas entering the interaction zone is transparent to the laser radiation and must be heated by thermal conduction from a pre-existing hot region of the flow in order that the plasma be self-sustaining. Such a mode obviously requires that an absorbing plasma be "ignited" by some means such as a spark or pulsed laser produced discharge.

In contrast, the solar sustained cesium plasma should be self starting. This is because the "cold" cesium vapor is not totally transparent to the sun's spectrum. As the unexcited vapor enters the solar radiation zone, strong dimer absorption will bring the gas up to a temperature high enough to populate the excited states and initiate energy deposition into the photoionization transitions. As this temperature is reached thermal dissociation will reduce the concentration of the dimers, dropping the dimer absorption coefficient to a value comparable to that of the bound-free transitions. The ground state photoionization absorption will also aid in this process but because of the narrow UV wavelength range in which it occurs it is not nearly as important to the overall energy balance as the dimer absorption which occurs in a broad wavelength range which would otherwise be relatively transparent (See Figure 1).

With the neglect of thermal conduction, Eq. (10) was integrated numerically along the direction of the incident solar radiation, z . The results of these computations are shown in Figures 3 and 4, assuming a solar concentration ratio of 3000.

Figure 3 shows the temperature, the fraction of incident radiation power remaining in the beam (transmitted power) and the fraction of incident radiation power contained in the plasma enthalpy flow (coupling efficiency) all as a function of z for chosen values for the input flow velocity and ambient cesium vapor pressure.

The coupling efficiency is equal to one minus the fractional power transmitted minus the fractional power radiated. It is seen to maximize at the same downstream location as does the temperature. In a heat engine application this location would then be the optimal point at which to extract the cesium plasma working fluid from the radiation interaction zone. This interaction length scales proportionally with the flow speed and will scale somewhat faster than inversely with the density because of the influence of the dimer. There is clearly a well defined tradeoff between peak coupling efficiency and peak plasma temperature: higher flow velocities yield higher coupling efficiencies but lower peak temperatures as one would expect. Since in a heat engine application the working cycle efficiency will generally increase with the input temperature of the working fluid the requirement for maximum overall efficiency will determine an optimal flow speed through the radiation interaction zone.

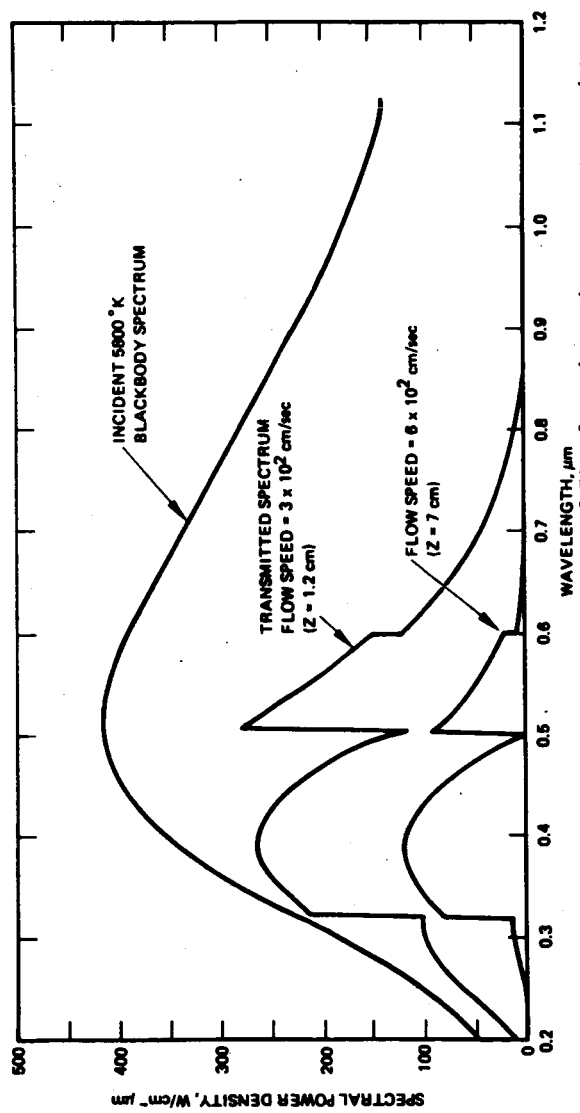


Fig. 4 Spectrum modification for the conditions of Fig. 3 at the maximum temperature points.

Figures 4a and 4b show how the incident solar spectrum has been modified by the plasma absorption at the maximum temperature points in Figures 3a and 3b. One can see the dominant influence of the photoionization transition on the short wavelength side and of the dimer transitions on the long wavelength side of the spectrum.

APPLICATION TO SOLAR DRIVEN MHD POWER GENERATION

MHD appears to be the only working cycle which can efficiently exploit the high temperatures generated in a solar sustained cesium plasma for the purposes of solar-electric conversion. A detailed analysis of a combined solar sustained cesium plasma MHD working cycle has not yet been carried out. We merely wish to point out in this section that the plasma parameters of a solar sustained cesium plasma are not incompatible with those of demonstrated MHD working fluids and that solar electric conversion efficiencies approaching 50% are therefore possible in principle with such a working cycle.

The most important plasma parameter for an MHD working fluid is its conductivity. From the literature on MHD power conversion (Ref. 8) one ascertains that the electrical conductivity of a one atmosphere pressure cesium plasma in the temperature range from $\sim 1500^\circ$ to 3000° is comparable to or higher than the conductivity of a 1% potassium seeded argon plasma. Conductivity values of $\sim 10^3$ mho/meter will attain in a one atmosphere cesium plasma at $\sim 3000^\circ\text{K}$. At a magnetic field of ~ 10 kilogauss, plasma conductivities of this order will require MHD duct lengths on the order of a meter (Ref. 9) for optimal extraction of the plasma enthalpy.

The other important parameter for an MHD plasma is the Hall parameter (electron-cyclotron frequency times mean-free time). The Hall parameter for a one atmosphere pressure solar-sustained cesium plasma at temperatures of $\sim 3000^\circ\text{K}$ has a value which is much greater than one for a ~ 10 kilogauss field. This condition permits the use of a Hall generator configuration wherein the induced current in the generator is in the direction of the plasma flow. An example of this type of MHD generator configuration is the disk generator design which does not require the use of segmented electrodes and has recently demonstrated a 15% enthalpy extraction efficiency (Ref. 10).

Whether or not a solar heated cesium MHD generator can approach the 50% overall conversion efficiency which results from the combination of a 40% efficient bottoming cycle with a 15% efficient MHD converter hinges on many additional engineering factors such as the effective coupling efficiency of solar radiation to the cesium plasma which ultimately must take into account specific geometrical constraints which impact the radiation interaction region, and in how well one can utilize the transmitted and re-radiated light in providing the heat of evaporation of the cesium, and the return of liquid cesium from the condenser to the evaporator in, for example, a Rankine super heat MHD working cycle.

REFERENCES

- ¹Zel'dovich, Ya. B. and Raizer, Yu. P., Physics of Shock Waves and High Temperature Hydrodynamic Phenomena, Vol. 1, Academic Press, N.Y., 1966.
- ²Hodges, R. E. M., Drummond, D. L., and Gallagher, A., "Extreme-Wing Line Broadening and C_8 -Inert-Gas Potentials," Phys. Rev., Vol. A6, Oct. 1972, pp. 1519-1544.
- ³Palmer, A. J., "Small-Sized Gain Modeling for Optical Pumping of the Alkali-Xenon and Alkali Dimer Laser Transitions," J.A.P., Vol. 47, July 1976, pp. 3088-3093.

- ⁴Herzberg, G., Spectra of Diatomic Molecules, Van Nostrand, New York, 1950, Appendix.
- ⁵Sorokin, P. P. and Lankard, J. R., "Emission Spectra of Alkali-Metal Molecules Observed with a Heat-Pipe Discharge Tube," J. Chem. Phys., Vol. 55, Oct. 1971, pp. 3810-3813.
- ⁶Lapp, M. and Harris, L. P., "Absorption Cross Sections of Alkali-Vapor Molecules," J. Quant. Rad. Trans., Vol. 6., March/April 1966, pp. 169-179.
- ⁷Raizer, Yu. P., "Supersonic Propagation of a Light Spark and Threshold Conditions for the Maintenance of Plasma by Radiation," JETP, Vol. 31, Dec. 1970, pp. 1148-1154.
- ⁸Lindley, B. C., "MHD Power Research in the United Kingdom," Engineering Aspects of MHD, Proceedings, 1960, p. 127.
- ⁹Rosa, R. J. and Kantrovitz, A., "MHD Energy Conversion Techniques," Direct Conversion of Heat to Electricity, edited by J. Kaye and J. Welsh, Wiley, N.Y., 1960.
- ¹⁰Kelpeis, J. and Hruby, V., "The Disk Geometry Applied to Open Cycle MHD Power Generation," Engineering Aspects of MHD, Proceedings, 1977, p. I.5.31.

PROGRAM LISTING

C SSP SOLAR SUSTAINED PLASMA

```

DIMENSION L(3),N(3),E(3),G(17)
DIMENSION WCU(200),WEU(200),DCW(200),DEW(200)
+ ,BETE(200),BETE(200),ALPHC(200),ALPHE(200)
DIMENSION BETA(100),PZ(100)
DIMENSION R(200),WU(200),WL(200),BET(200),
+ DW(200),ALPH(200),BET3(200),ALPHB(200),DBW(200),WBU(200),
+ ALPH(100),BETAB(100),RRCQ(100)
REAL ME,M1,N1T,KF,KB,LAMDA,L,N,LOGNE,NR
INTEGER Q
REAL KX,KA,KDB,KDE,KDC

```

C DATA FOR CS2

```

GU=1.;GL=1.;GR=12.;GG=4.
WK3=21855
WR2=11736
WK=11.178E3
RO=30.
RZERO=5.5
QU1=10
DEL=01./FLOAT(NUM)
NB=19*NUM
NBN=NB-1
DNR=1.E-5
AU=.59E8
MU=55.473
WA=34.
WC=15
WE=30
WB=34.2
WX=42
JC=500
JE=5259
JB=1510
JA=5100
JX=3600
REE=5.7E-3
REC=5.7E-3
REB=4.47E-3
REA=5.25E-3
REX=4.47E-3
GE=1.22E7*WE*SQR(MU/DE)
GC=1.22E7*WC*SQR(MU/DC)
GB=1.22E7*WB*SQR(MU/DB)
GA=1.22E7*WA*SQR(MU/DA)
GX=1.22E7*WX*SQR(MU/DX)

```

C COMPUTE R(I) AND MORSE POTENTIALS

```

DO 2 I=1,NB
R(I)=RZERO+FLOAT(I)*DEL
WEU(I)=DE*(1.-EXP(-BE*(R(I)*.53E-8-REE)))*2+(WR3-DE)
WCU(I)=DC*(1.-EXP(-BC*(R(I)*.53E-8-REC)))*2+(WR2-DC)
WBU(I)=DB*(1.-EXP(-BB*(R(I)*.53E-8-REB)))*2+(WR-DB)
WU(I)=DA*(1.-EXP(-BA*(R(I)*.53E-8-REA)))*2+(WR-DA)
WL(I)=DX*(1.-EXP(-BX*(R(I)*.53E-8-REX)))*2+(-DX)
2 CONTINUE

```

C COMPUTE LINE SHAPE DERIVITIVES

```

DO 65 I=1,NBM
K=1
31 DW(I)=(WU(I+K)-WL(I+K)-(WU(I)-WL(I)))/FLOAT(K)
IF (FLOAT(K)*ABS(DW(I))-DWR) 36,35,35
36 K=K+1
IF (I+K-NB) 37,37,38
37 GO TO 31
38 DW(I)=DWR
35 CONTINUE
J=1
161 DEW(I)=(WEU(I+J)-WL(I+J)-(WEU(I)-WL(I)))/FLOAT(J)
IF (FLOAT(J)*ABS(DEW(I))-DWR) 166,165,165
166 J=J+1
IF (I+J-NB) 167,167,168
167 GO TO 161
168 DEW(I)=DWR
165 CONTINUE
J=1
261 DCW(I)=(WCU(I+J)-WL(I+J)-(WCU(I)-WL(I)))/FLOAT(J)
IF (FLOAT(J)*ABS(DCW(I))-DWR) 266,265,265
266 J=J+1
IF (I+J-NB) 267,267,268
267 GO TO 261
268 DCW(I)=DWR
265 CONTINUE
J=1
61 DBW(I)=(WBU(I+J)-WL(I+J)-(WBU(I)-WL(I)))/FLOAT(J)
IF (FLOAT(J)*ABS(DBW(I))-DWR) 66,65,65
66 J=J+1
IF (I+J-NB) 67,67,68
67 GO TO 61
68 DBW(I)=DWR
65 CONTINUE
DATA H/1.,1.26,1.39,1.60,1.85,1.93,2.14,2.17/
DATA L/0,1,2,0,1,2,0,3/
DATA E/0,1.43,1.80,2.30,2.71,2.80,3.00,3.03/

```

C INPUT

```

WRITE (5,50)
50 FORMAT (2X,2HTO,2X,2HZF,2X,2HDZ,2X,6HIPRINT,2X,4HZMAX,
+2X,2HCF,2X,4HTEMP)
ACCEPT*,TO,ZF,DZ,IPRINT,ZMAX,CF,TEMP
AF=0.222;FNO=1.6

```

C COMPUTE VAPOR PRESSURE AND DENSITY

```

PRES=10**((11.0531-1.35*ALOG10(TO))-4041/TO)
CSO=2.7E10*(273/TO)*PRES

```

C COMPUTE INPUT BLACK BODY SPECTRUM

```

DO 33 Q=1,100
LAMD=.25+Q*.01
25 PZ(Q)=3.74E8*LAMD**-5*(EXP(1.44E4/(LAMD*5800))-1.)**-1
PT=PT+PZ(Q)*.01E-4
33 CONTINUE
HVAP=U*CSO*11.2E-20/PT
WRITE (5,52) PRES,CSO,HVAP
52 FORMAT (2X,'PRESSURE=',E10.3,2X,'CSO=',E10.3,2X,'HVAP=',E10.3)
WRITE (5,40)
40 FORMAT (4X,1HZ,10X,4HTEMP,7X,4HCONV,7X,4HCOND,4X,3HRAD,7X,2HCT)
RT=0

```

C Z STEP

```

20 ISTEP=ISTEP+1
Z=Z+DZ
IF (Z-ZMAX) 21,21,22
21 CONTINUE

```

C COMPUTE ATOMIC AND MOLECULAR EQUILIBRIUM POPULATION DENSITIES

```

DO 421 M=1,50
429 RATO=RAT;WZZO=WZZ
T=TEMP*(1/1.16E4)
N1=CSO*TO/TEMP
NR=N1*EXP(-E(2)/T)*GR/GG
KX=3.47E-7*EXP(5236.7/TEMP)*1/2.75E16*(TEMP/273)
KA=8E-23*EXP(.62/T)
KDB=3E-23*EXP(DB*1.24E-4/T)
KDC=3E-23*EXP(DC*1.24E-4/T)
KDE=3E-23*EXP(DE*1.24E-4/T)
DIMX=N1*KX*N1
DIMA=N1*KA*NR
DINB=N1*KDB*NR
DINC=N1*KDC*NR
DIME=N1*KDE*N1*EXP(-E(5)/T)*GR/GG
IF (DIMX-N1) 16,16,17

```

```

17 DIMX=N1
16 CONTINUE
  IF (DIMA-NR) 23,23,24
24 DIMA=NR
23 CONTINUE
  IF (DIME-NR) 197,197,193
193 DIME=NR
197 CONTINUE
  IF (DIMC-NR) 297,297,293
293 DIMC=NR
297 CONTINUE
  IF (DIMB-NR) 97,97,93
93 DIMB=NR
97 CONTINUE

```

```

C COMPUTE RESONANCE LINE ABSORPTION COEFFICIENT
  BETR=N1*AU/(3*3.14*WR**2*1E10)
  + *GU/GL

```

```

C COMPUTE ABSORPTION & EMISSION COEF VS R

```

```

  DO 10 I=1,NBM
    BET(I)=(0.5*AU*R(I)**2*DIMX*(0.53E-8)**3*(1/KX)/(WU(I)-WL(I))**2
  + )*EXP(-WL(I)*1.24E-4/T)*DEL*(1/3E10)/ABS(DW(I))*GU/GG
  + *((WU(I)-WL(I))/WR)**3
    ALPH(I)=3.14*AU*R(I)**2*DIMA*(.53E-8)**3*(1/KA)*EXP(-(WU(I)
  + -WR)*1.24E-4/T)*DEL*(WU(I)-WL(I))*1.24E-4*GU/GR
  + *((WU(I)-WL(I))/WR)**3
    IF (BET(I)-BETR) 94,7,7
  7 BET(I)=BETR
  94 CONTINUE
    BETE(I)=(.05*AU*R(I)**2*DIMX*(0.53E-8)**3*(1/KX)/(WEU(I)-WL(I))**2
  + )*EXP(-WL(I)*1.24E-4/T)*DEL*(1/3E10)/ABS(DEW(I))*GU/GG
  + *((WEU(I)-WL(I))/WR2)**3
    IF ((WEU(I)-WR2)*1.24E-4/T-23) 406,406,407
  407 ALPH(I)=0; GO TO 408
  406 ALPH(I)=.314*AU*R(I)**2*DIME*(.53E-8)**3*(1/KDE)*EXP(-(WEU(I)
  + -WR2)*1.24E-4/T)*DEL*(WEU(I)-WL(I))*1.24E-4*GU/GR
  + *((WEU(I)-WL(I))/WR2)**3
  408 CONTINUE
    IF (BETE(I)-BETR) 410,495,495
  495 BETE(I)=BETR
  410 CONTINUE
    BETC(I)=(.05*AU*R(I)**2*DIMX*(0.53E-8)**3*(1/KX)/(WCU(I)-WL(I))**2
  + )*EXP(-WL(I)*1.24E-4/T)*DEL*(1/3E10)/ABS(DCW(I))*GU/GG
  + *((WCU(I)-WL(I))/WR)**3
    IF ((WCU(I)-WR)*1.24E-4/T-23) 506,506,507
  507 ALPH(I)=0; GO TO 508
  506 ALPH(I)=.314*AU*R(I)**2*DIMC*(.53E-8)**3*(1/KDC)*EXP(-(WCU(I)
  + -WR)*1.24E-4/T)*DEL*(WCU(I)-WL(I))*1.24E-4*GU/GR
  + *((WCU(I)-WL(I))/WR)**3

```

```

508 CONTINUE
  IF (BETC(I)-BETR) 510,595,595
595 BETC(I)=BETR
510 CONTINUE
  BETB(I)=(0.5*AU*(I)**2*DIMA*(0.53E-8)**3*(1/KK)/(WBU(I)-WL(I))**2
+ )*EXP(-WL(I)*1.24E-4/T)*DEL*(1/3E10)/ABS(DBW(I))*GU/GG
+*((WBU(I)-WL(I))/WR)**3
  IF ((WBU(I)-WR)*1.24E-4/T-23) 306,306,307
307 ALPHB(I)=0; GO TO 308
306 ALPHB(I)=3.14*AU*(I)**2*DIMA*(.53E-8)**3*(1/KDB)*EXP(-(WBU(I)
+-WR)*1.24E-4/T)*DEL*(WBU(I)-WL(I))*1.24E-4*GU/GR
+*((WBU(I)-WL(I))/WR)**3
308 CONTINUE
  IF (BETB(I)-BETR) 10,95,95
95 BETB(I)=BETR
10 CONTINUE
  RD=0
  WZ=0
  BAV=0

```

C COMPUTE ELECTRON DENSITY, RECOMBINATION RADIATION, & BOUND FREE ABSORPTION

```

3 NE=2**-.5*30**-.5*EXP(-3.89/(2*T))*SQRT(N1)*1E10
  RRC=0
  DO 19 J=1,8
    RRC=RRC+1.252E-33*NE*T**-.5*NE*2*(2*L(J)+1)/N(J)**5
    IF (J-1) 3,8,19
3 RRC=.025*RRC
19 CONTINUE
  RRCT=0
  DO 15 Q=1,100
    BETAD(Q)=0
    ALPHD(Q)=0
    LAMDA=.25+Q*.01
    KB=0
    RRCQ(Q)=0
    DO 72 J=1,8
      IF ((3.39-E(J))-(1.24/LAMDA)) 45,45,72
45 CONTINUE
      KB=KB+(2*L(J)+1)/N(J)**5*EXP(-E(J)/T)*N1
      RRCQ(Q)=RRCQ(Q)+(2*L(J)+1)/N(J)**5*EXP(-E(J)/T)*N1*.01E-4
      +*7.9E-18*(3.89*LAMDA/1.24)**3*3.74E8*LAMDA**-5*
      +(EXP(1.44E4/(LAMDA*TEMP))-1.))**-1
      IF (J-1) 9,9,72
9 KB=.025*KB; RRCQ(Q)=.025*RRCQ(Q)

```

C COMPUTE ABSORPTION & EMISSION COEF VS WAVELENGTH

```

72 CONTINUE
  FREQ=1E4/LAMDA
  DO 191 J=1,NBM
    IF (FREQ-(WU(J)-WL(J)+ABS(DW(J)/2.))) 90,90,91
  90 IF (FREQ-(WU(J)-WL(J)-ABS(DW(J)/2.))) 91,92,92
  92 BETAD(Q)=BETAD(Q)+BET(J)
    ALPHD(Q)=ALPHD(Q)+ALPH(J)*.01E4/(LAMDA**2*ABS(DW(J)))
  91 CONTINUE
    IF (FREQ-(WEU(J)-WL(J)+ABS(DEW(J)/2.))) 290,290,291
  290 IF (FREQ-(WEU(J)-WL(J)-ABS(DEW(J)/2.))) 291,292,292
  292 BETAD(Q)=BETAD(Q)+BETE(J)
    ALPHD(Q)=ALPHD(Q)+ALPHE(J)*.01E4/(LAMDA**2*ABS(DEW(J)))
  291 CONTINUE
    IF (FREQ-(WCU(J)-WL(J)+ABS(DCW(J)/2.))) 390,390,391
  390 IF (FREQ-(WCU(J)-WL(J)-ABS(DCW(J)/2.))) 391,392,392
  392 BETAD(Q)=BETAD(Q)+BETC(J)
    ALPHD(Q)=ALPHD(Q)+ALPHC(J)*.01E4/(LAMDA**2*ABS(DCW(J)))
  391 CONTINUE
    IF (FREQ-(WBU(J)-WL(J)+ABS(DBW(J)/2.))) 190,190,191
  190 IF (FREQ-(WBU(J)-WL(J)-ABS(DBW(J)/2.))) 191,192,192
  192 BETAD(Q)=BETAD(Q)+BETB(J)
    ALPHD(Q)=ALPHD(Q)+ALPHB(J)*.01E4/(LAMDA**2*ABS(DBW(J)))
  191 CONTINUE
    BETA(Q)=7.9E-18*(3.39*LAMDA/1.24)**3*(KB+KF)+BETAD(Q)
    IF (ALPHD(Q)-1.E-11) 301,301,303
  301 ALPHD(Q)=0
  303 RD=RD+ALPHD(Q)*1.6E-19; RRCT=RRCT+RRCQ(Q)
    WZ=WZ+PZ(Q)*BETA(Q)*.01E-4
  15 CONTINUE

```

C COMPUTE ENERGY DEPOSITION & CONVECTIVE & CONDUCTIVE ENERGY LOSS

```

  RADIUS=SQRT(AF/3.14)+ABS(ZF-Z)/(2*FNO)
  WZZ=WZ*CF*AF/(3.14*RADIUS**2)
  VB=(930*(TEMP-TO)/TO*RADIUS/2)**.5
  RAD=RRCT/1.44+RD*1.2
  CONV=1.5*N1*1.4E-23*(TEMP-TO)/RADIUS*VB
  COND=15E-5*(TEMP-TO)/RADIUS**2
  RAT=RAD+CONV+COND

```

C COMPUTE PLASMA TEMPERATURE

```

  IF (TEMP-TO) 430,430,431
  430 TEMP=TO;GO TO 422
  431 IF (RAT) 419,421,419
  419 IF ((RAT-WZZ)/ABS(RAT-WZZ)-(RATO-WZZO)/ABS(RATO-WZZO)) 422,420,420
  420 IF (RAT-WZZ) 440,441,441
  440 DTEMP=200;GO TO 442
  441 DTEMP=-200

```

442 TEMP=TEMP+DTEMP

441 CONTINUE

442 CONTINUE

RT=RT+RAT*DZ

PTZ=0

BAV=0

C COMPUTE MODIFIED INPUT SPECTRUM

DO 23 Q=1,100

LAMDA=.25+Q*.01

PZ(Q)=PZ(Q)*EXP(-BETA(Q)*DZ)

PTZ=PTZ+PZ(Q)*.01E-4

BAV=BAV+BETA(Q)*PZ(Q)*.01E-4

31 FORMAT(4(E11.3))

28 CONTINUE

C OUTPUT

IF (ISTEP/IPRINT-FLOAT(ISTEP)/FLOAT(IPRINT)) 20,30,20

30 CONTINUE

CT=PTZ/PT

CQ=(PT-(PTZ+RT))/PT

CQV=CQ+HVAP

DAV=PTZ/BAV

WRITE (5,*) DIMX

WRITE (5,30) Z,TEMP,CONV,COND,RAD,CT

30 FORMAT (5(E11.3))

GO TO 20

22 WRITE (5,200)

200 FORMAT(3X,19H>0, GO ON---<0, END)

ACCEPT*,Y

IF(Y) 70,70,42

42 WRITE (5,250)

250 FORMAT(2X,23HNEW VALUES: DZ, ZMAX, IPRINT)

ACCEPT*,DZ,ZMAX,IPRINT

IF (IPRINT) 210,212,212

210 WRITE (5,32)

32 FORMAT(2X,5HLAMDA,6X,5HTRANS,6X,4HRATQ)

DO 214 Q=1,100,2

LAMDA=.25+Q*.01

RATQ=RRQ(Q)+ALPHQ(Q)*1.6E-19

CROS=BETA(Q)*(1E16/DIMX)

TRANS=PZ(Q)/(3.74E8*LAMDA**5*(EXP(1.44E4/(LAMDA*5000))-1.))**(-1)

214 WRITE (5,81) LAMDA,TRANS,RATQ

GO TO 70

212 CONTINUE

ISTEP=J

GO TO 20

70 CONTINUE

END